
复杂系统临界现象与标度性

陈晓松

北京师范大学系统科学学院

2020.06.24—华中师范大学

报告内容

- 临界现象研究的回顾及现状
- 统计系综的本征微观态方法与相变临界现象及标度性
- 不同维数平衡态Ising模型的本征微观态与铁磁相变
- 地球系统温度涨落的本征微观态
- 漏斗颗粒流速度场的标度性与Beveloo定律
- 总结

人类科学研究两个主要方向

- 还原论：例如：探索物质的深层次结构及相互作用
物质 → 分子 → 原子 → 质子，中子，电子 → 夸克....
- 系统论（统计物理学...）：
大量个体组成的复杂系统的构造和演化规律

超越个体，呈现合作、有序、聚集等

统计物理学：

- **Statistical physics** is the branch of [physics](#) that uses methods of [probability theory](#) and [statistics](#), and particularly the [mathematical](#) tools for dealing with large populations and approximations, in solving physical problems. It can describe a wide variety of fields with an inherently [stochastic](#) nature. Its applications include many problems in the fields of physics, [biology](#), [chemistry](#), [neurology](#), and even some social sciences, such as [sociology](#). Its main purpose is to clarify the properties of matter in aggregate, in terms of physical laws governing atomic motion.^[1]

微观性质 → 集体、涌现、全局的性质

More is different

多者异也！

Philip W. Anderson

(1972)



……将万事万物还原成简单的基本规律，并不意味着从这些规律出发重建宇宙的能力……

不能依据少数粒子的性质简单外推出多粒子复杂集聚体的行为。相反，在复杂体系的每一个层次会呈现全新的性质。研究、理解此类新行为，就其基础性而言，与其他研究相比毫不逊色。

统计物理：绚丽多姿的世界——我们身边的科学

- 经典系统：气体、液体、固体
 - 量子系统：金属和半导体中的电子、光子、声子等
 - 新物态：超导、超流、玻色凝聚、拓扑量子序
 - 人工量子结构：相干量子器件、量子计算、量子器件
 - 复杂系统：生物、生态系统、网络系统、社会系统、气候系统、环境系统等
- 特点：非平衡态、有限系统

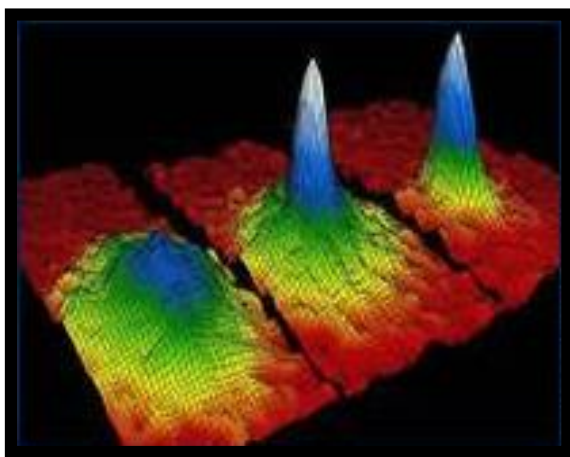
经典、量子系统的聚集与相变

聚集体

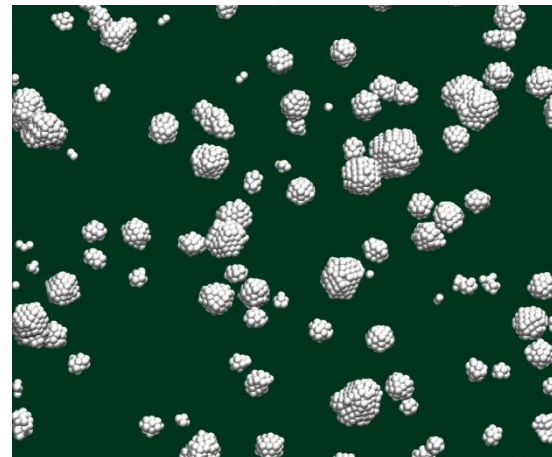
- 是相互作用多组元的复杂体系
- 具有超越个体行为的整体特征：合作、聚集



冰花



玻色爱因斯坦凝聚

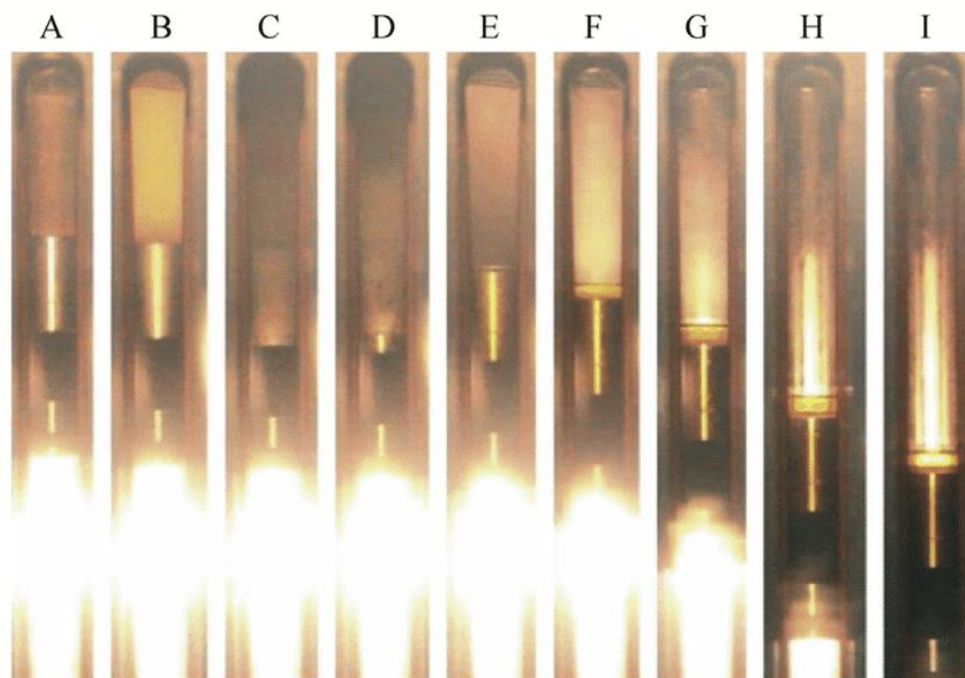


纳米微观结构

临界现象研究的里程碑

- Andrews发现CO₂ 的临界点 (1869)
- 范德瓦尔斯理论 (1873) (第一个理论方面诺贝尔物理学奖)
- Onsager二维伊辛模型的精确解 (1944)
- K. G. Wilson重整化群理论 (1971) (1982年诺贝尔物理学奖)

临界乳光 (1869首次在二氧化碳实验被观测)



系统的临界点

- 水

$T_c = 374.15$ 摄氏度, $P_c = 221.2$ bar

- 二氧化碳

$T_c = 31.04$ 摄氏度, $P_c = 73$ bar

爱因斯坦的临界乳光理论

Theory of Critical Opalescence



- Einstein returned to the problem of thermodynamic fluctuations, giving a treatment of the density variations in a fluid at its critical point. Ordinarily the density fluctuations are controlled by the second derivative of the free energy with respect to the density. At the critical point, this derivative is zero, leading to large fluctuations. The effect of density fluctuations is that light of all wavelengths is scattered, making the fluid look milky white.

复杂系统的相变

生物系统的相变：

Nature, 483, 336 (2012)

Phase transitions in the assembly of multivalent signalling proteins

• [Pilong Li](#) et. Al.

Ecology Letters, (2018)21: 905–919

Indicators of transition in biological systems

C. F. Clements et. al.

气候系统：

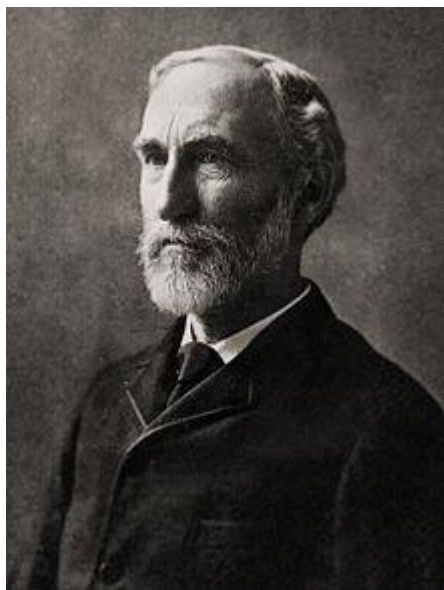
PNAS, 105, 1786 (2008)

Tipping elements in the Earth's climate system

T. M. Lenton et al.

巨大挑战：非平衡，系统有限，序参量不能确定

统计物理的J. W. Gibbs (1839-1903) 系综理论



an **ensemble** (also **statistical ensemble**) is an idealization consisting of a large number of virtual copies (sometimes infinitely many) of a [system](#), considered all at once, each of which represents a possible state that the real system might be in.

a **microstate** is a specific microscopic configuration of a [thermodynamic system](#)

• **Statistical mechanics**: [statistical ensemble](#), [phase space](#), [chemical potential](#), [Gibbs entropy](#), [Gibbs paradox](#)

Thermodynamic ensembles:

- NVE [Microcanonical](#)
- NVT [Canonical](#)
- μVT [Grand canonical](#)

平衡态系统的统计系综微观态分布

微正则系综

For an isolated system at equilibrium, all microstates are equally probable.

$$\Rightarrow p_i(E) = \begin{cases} \frac{1}{\Omega(E)} = \text{const} & E - \delta E \leq E_i \leq E \\ 0 & \text{otherwise} \end{cases}$$

正则系综:

$$p_i = \frac{1}{Z} e^{-\beta E_i} \quad \text{Boltzmann distribution}$$

$$Z = \sum_i e^{-\beta E_i} \quad \text{partition sum}$$

巨正则系综

:

$$p_i = \frac{1}{Z_G} e^{-\beta(E_i - \mu N_i)} \quad \text{grandcanonical prob. distribution}$$

where

$$Z_G = \sum_i e^{-\beta(E_i - \mu N_i)} \quad \text{grandcanonical partition sum}$$

复杂系统研究中的挑战

- 系统一般处于非平衡态、不断演化，系统的系综微观态分布未知
- 系统的序参量未知，现有相变临界现象理论建立在序参量已知的基础之上

统计系统的本征微观态理论

Sci. China Phys. Mech.&Astron. 62, 990511 (2019)

微观态:

In a complex system composed of N agents, the states of agent can be measured from its experimental investigations or computer simulations. From the measurements at times $t = 1, 2, \dots, M$ in sequence, we obtain a series of states $S_i(t)$ of agents $i = 1, 2, \dots, N$.

The microstate of the complex system at t can be described by an N -dimensional normalized vector

$$\mathbf{S}(t) = \frac{1}{\sqrt{\sum_{i=1}^N S_i(t)^2}} \begin{bmatrix} S_1(t) \\ S_2(t) \\ \vdots \\ S_N(t) \end{bmatrix}, \quad (1)$$

统计系综矩阵

which satisfies the condition $\bar{\mathbf{S}}(t)^T \cdot \bar{\mathbf{S}}(t) = 1$. Using microstates $\bar{\mathbf{S}}(t)$ at $t = 1, 2, \dots, M$, we can compose a statistical ensemble characterize by an $N \times M$ matrix \mathbf{A} with elements

$$A_{it} = \frac{1}{\sqrt{M}} \frac{S_i(t)}{\sqrt{\sum_{i=1}^N S_i(t)^2}}, \quad (2)$$

which satisfies the condition $\sum_{t=1}^M \sum_{i=1}^N A_{it}^2 = 1$.

微观态关联矩阵

The correlation between microstates at t and t' is defined by their vector product as

$$C_{tt'} = \mathbf{S}(t)^T \cdot \mathbf{S}(t') = \frac{\sum_{i=1}^N S_i(t) S_i(t')}{\sum_{i=1}^N S_i(t)^2}. \quad (3)$$

With $C_{tt'}$ as its elements, we get an $M \times M$ correlation matrix of microstate

$$\mathbf{C} = M \mathbf{A}^T \cdot \mathbf{A}, \quad (4)$$

whose trace is equal to M .

关联矩阵的本征矢量

From \mathbf{A} , we can obtain also an $N \times N$ matrix

$$\mathbf{K} = \mathbf{M} \mathbf{A} \cdot \mathbf{A}^T, \quad (5)$$

whose trace is equal to M also.

Using eigenvectors \mathbf{V}_t of \mathbf{C} , we can get an $M \times M$ unitary matrix

$$\mathbf{V} = [\mathbf{V}_1 \mathbf{V}_2 \dots \mathbf{V}_M]. \quad (6)$$

The eigenvectors \mathbf{U}_i of \mathbf{K} composes an $N \times N$ unitary matrix as

$$\mathbf{U} = [\mathbf{U}_1 \mathbf{U}_2 \dots \mathbf{U}_N]. \quad (7)$$

统计系综矩阵的分解

$$\mathbf{A} = \mathbf{U} \cdot \mathbf{\Sigma} \cdot \mathbf{V}^T, \quad (10)$$

where $\mathbf{\Sigma}$ is an $N \times M$ diagonal matrix with elements

$$\Sigma_{ij} = \begin{cases} \sigma_i, & i = j \leq r, \\ 0, & \text{otherwise,} \end{cases} \quad (11)$$

with $r = \min(N, M)$. Now, we can rewrite the correlation matrices \mathbf{C} and \mathbf{K} as

$$\mathbf{C} = \mathbf{V} \cdot \mathbf{\Sigma}^T \mathbf{\Sigma} \cdot \mathbf{V}^T, \quad (12)$$

$$\mathbf{K} = \mathbf{U} \cdot \mathbf{\Sigma} \mathbf{\Sigma}^T \cdot \mathbf{U}^T. \quad (13)$$

统计系综矩阵的分解

According to Eq.(10), we can decompose the ensemble matrix \mathbf{A} as

$$\mathbf{A} = \sum_{I=1}^r \sigma_I \mathbf{U}_I \otimes \mathbf{V}_I . \quad (14)$$

The eigenvalues satisfy the normalization condition

$$\text{Tr}(\mathbf{C}) = \text{Tr}(\mathbf{K}) = \sum_{I=1}^r |\sigma_I|^2 = 1 . \quad (15)$$

We can interpret $|\sigma_I|^2$ as the probability of $\mathbf{U}_I \otimes \mathbf{V}_I$ in the statistical ensemble \mathbf{A} .

本征微观态:

Using all microstates $\mathbf{S}(t)$ and an eigenvector \mathbf{V}_I , we can define an N -dimensional eigen microstate [6]

$$\mathbf{S}^E(I) = \sum_{m=1}^M \bar{\mathbf{S}}(m) V_{mI} . \quad (14)$$

The i -th component of $\mathbf{S}^E(I)$ is

$$\mathbf{S}_i^E(I) = \sum_{m=1}^M A_{im} V_{mI} = (\mathbf{A} \cdot \mathbf{V})_{iI} = (\mathbf{U} \cdot \mathbf{\Sigma})_{iI} . \quad (15)$$

Therefore, we have

$$\mathbf{S}^E(I) = \begin{cases} \sigma_I \mathbf{U}_I , & I \leq r, \\ 0 , & \text{otherwise.} \end{cases} \quad (16)$$

Between different eigen microstates, there is no correlation since $\mathbf{S}^E(I)^T \cdot \mathbf{S}^E(J) = 0$ for $I \neq J$.

原始微观态可看作本征微观态的线性叠加

We can expand original microstates by eigen microstates as

$$\bar{\mathbf{S}}(t) = \sum_{I=1}^M V_{tI} \mathbf{S}^E(I) = \sum_{I=1}^r \sigma_I V_{tI} \mathbf{U}_I. \quad (17)$$

本征微观态的权重因子：

$$w_{\mathbf{I}} = \sigma_{\mathbf{I}}^2$$

本征微观态的凝聚与系统相变：

系综微观态无局域化时： $\mathbf{M}, \mathbf{N} \rightarrow \infty$ ，权重因子 $\rightarrow 0$

若 $\mathbf{M}, \mathbf{N} \rightarrow \infty$ ，权重因子 \rightarrow 有限值

统计系综中本征微观态出现了凝聚

系统发生相变，新相由该本征微观态完全描述

本征值（权重因子）的有限尺度标度性

For a continuous phase transition, σ_1 changes always continuously. For a complex system with critical temperature T_c , we define the reduced temperature $t = (T - T_c)/T_c$. In the asymptotic region with $|t| \ll 1$, there is a finite-size relation of eigenvalues [6]

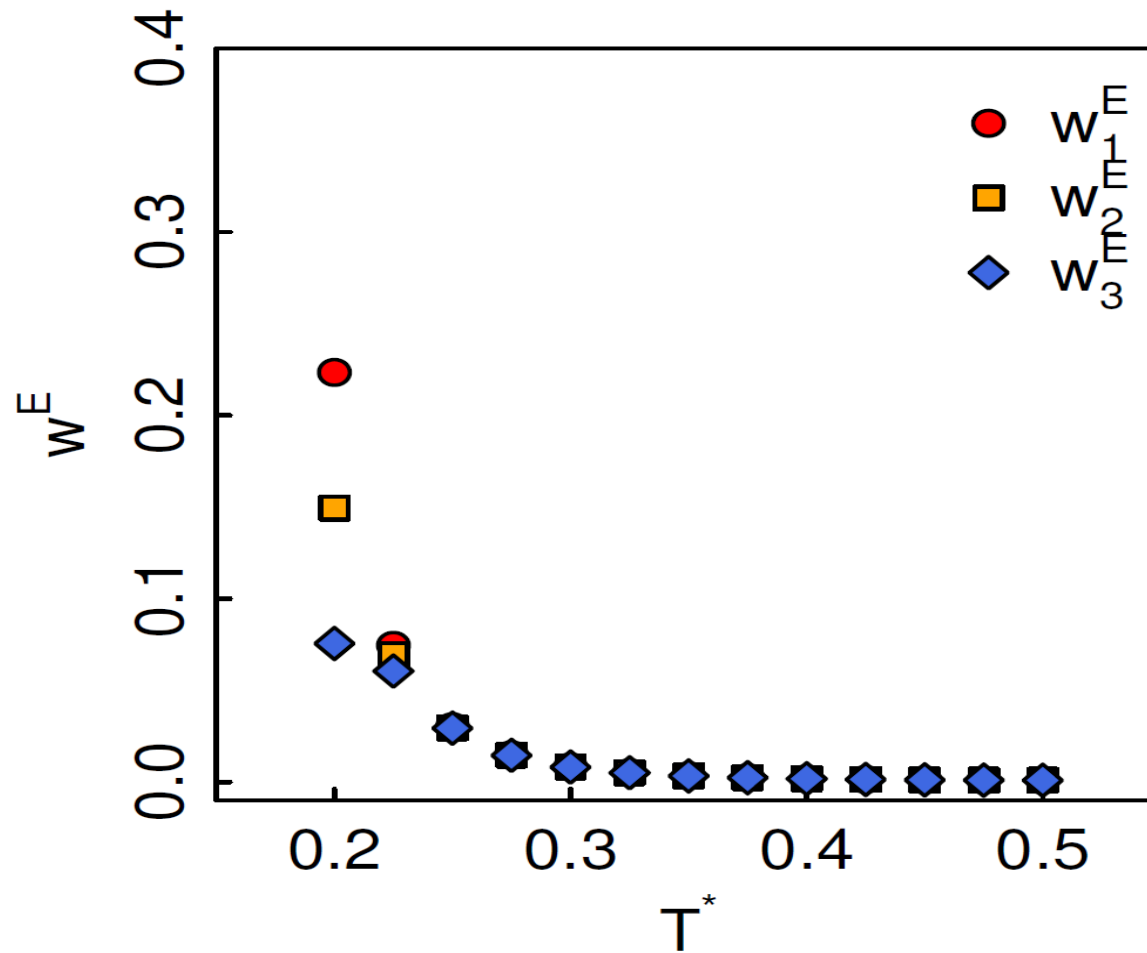
$$\sigma_I(T, N) = N^{-\beta/d\nu} f_I(tN^{1/d\nu}), \quad (18)$$

where β is the critical exponent of order parameter and ν is the critical exponent of correlation length. The con-

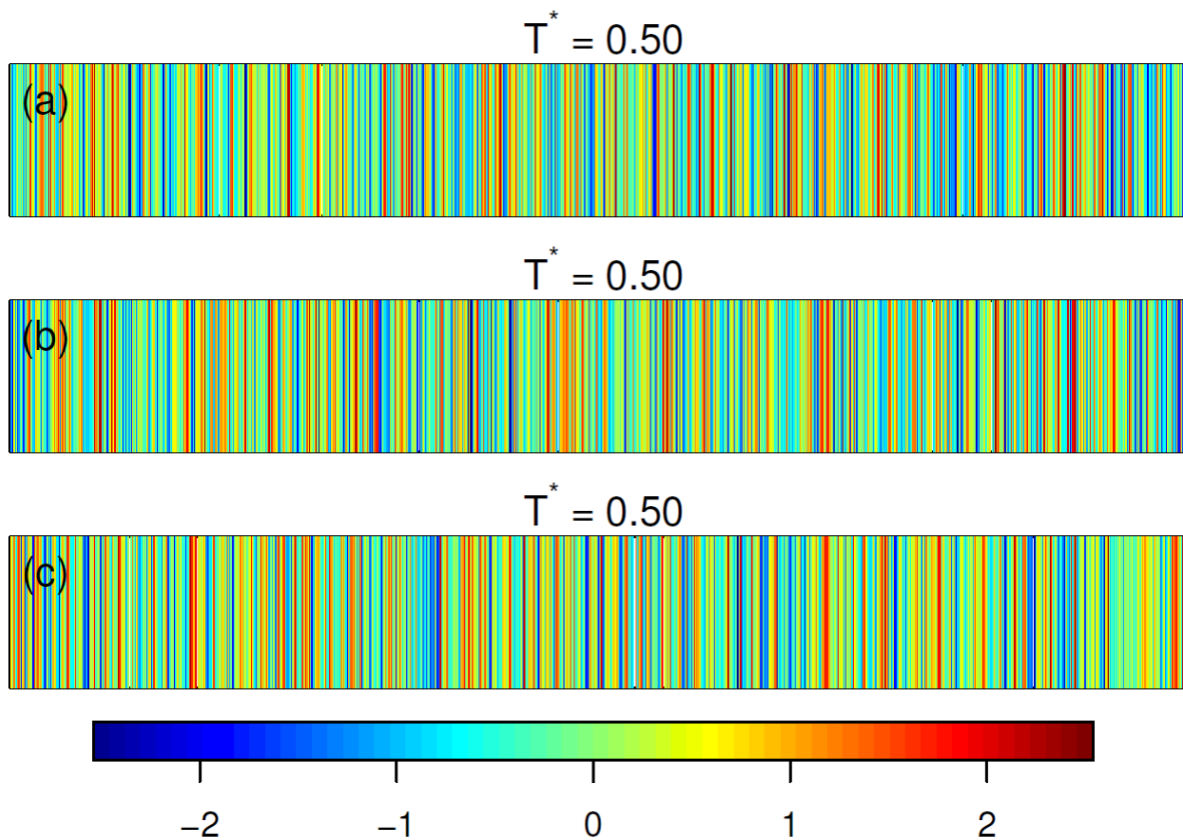
本征微观态理论的优势：

- 不局限于平衡态系统
- 可自然确定相变及序参量
- 比较适用有限的复杂系统

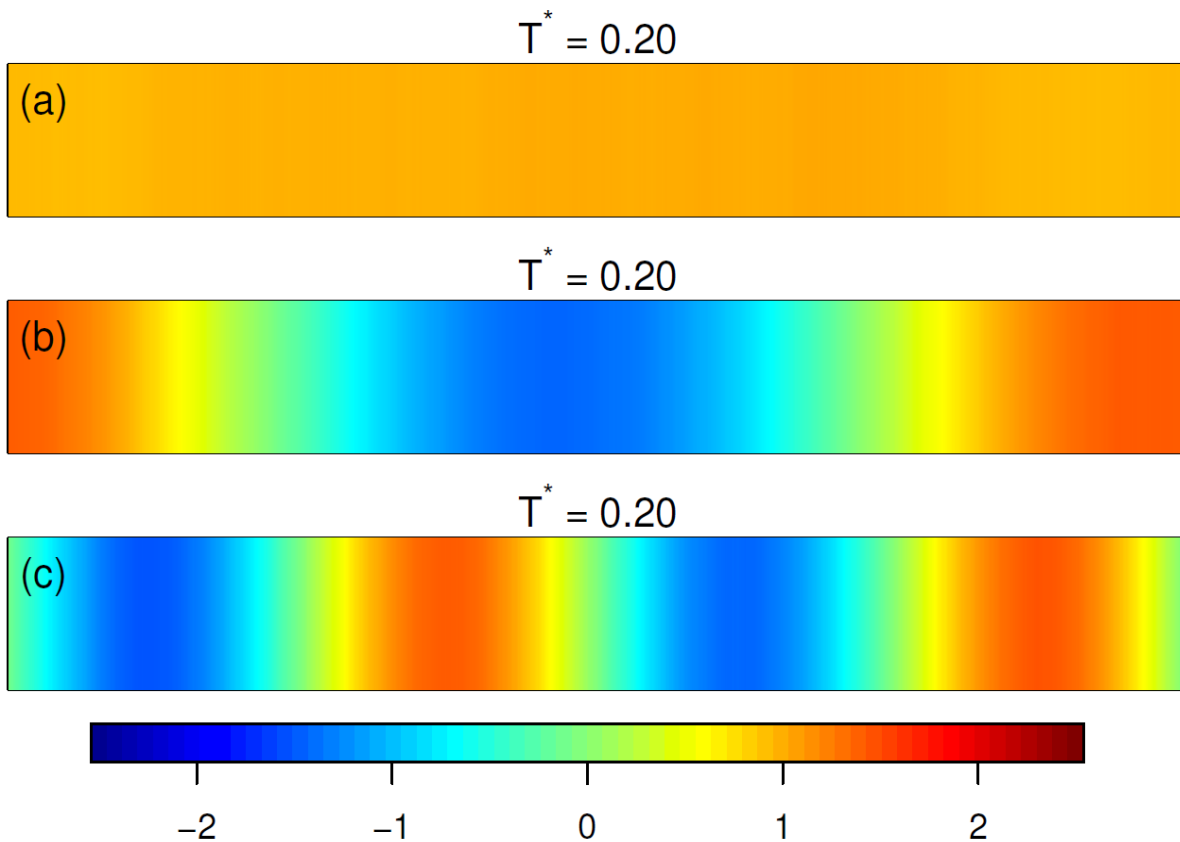
一维 Ising 模型平衡态本征微观态的权重因子:



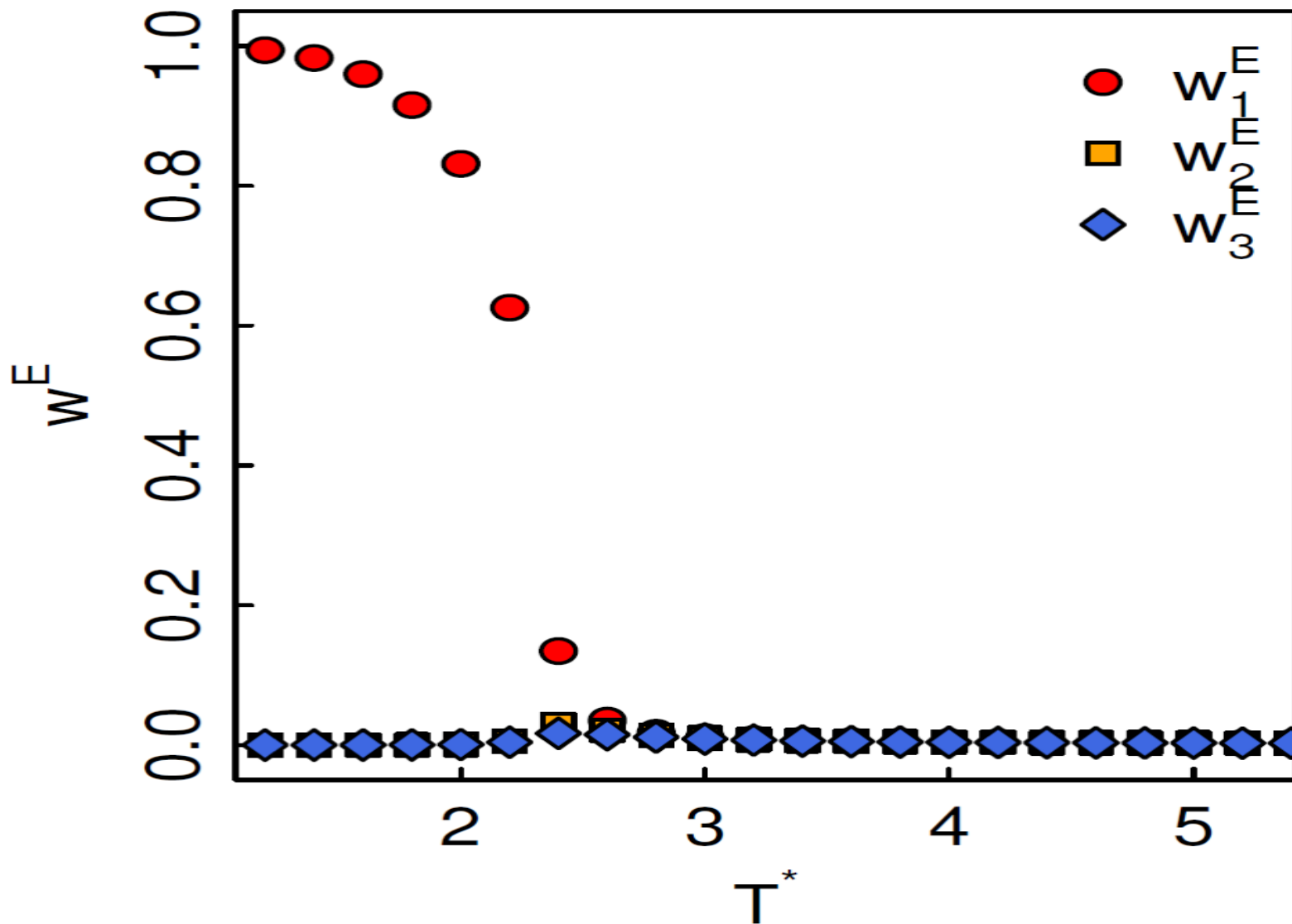
一维Ising模型的前3大本征微观态：



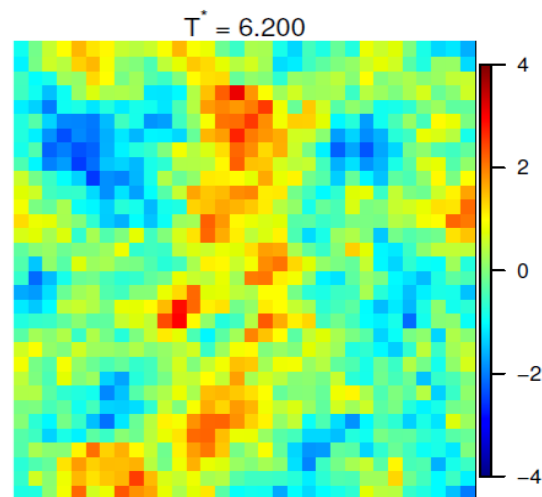
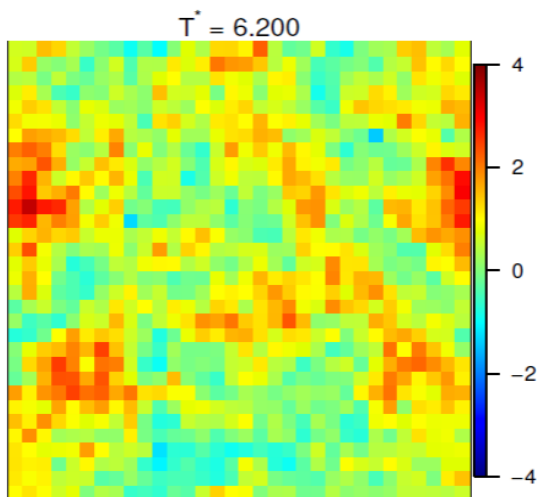
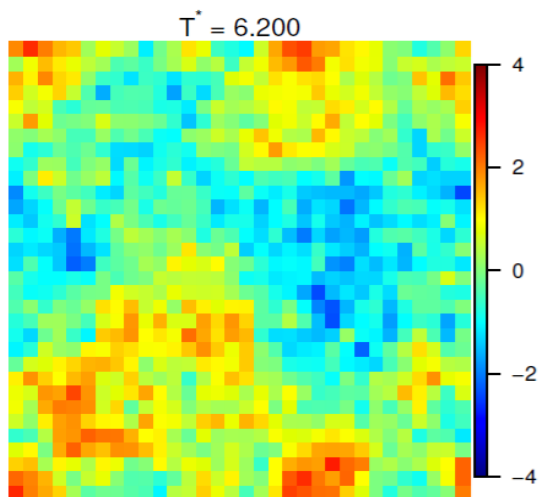
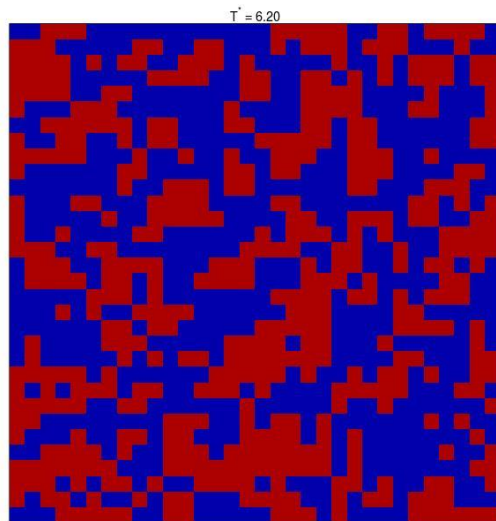
一维Ising模型前3大本征微观态



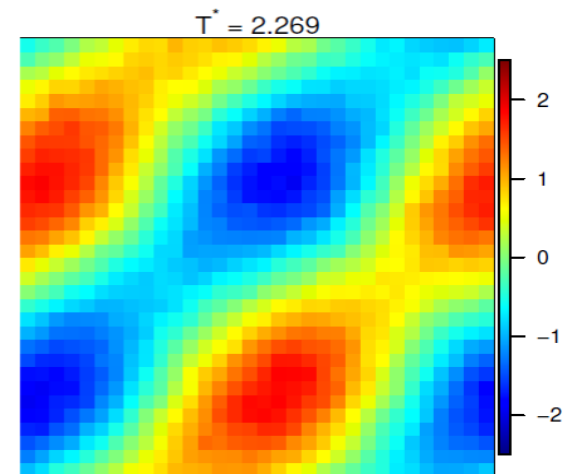
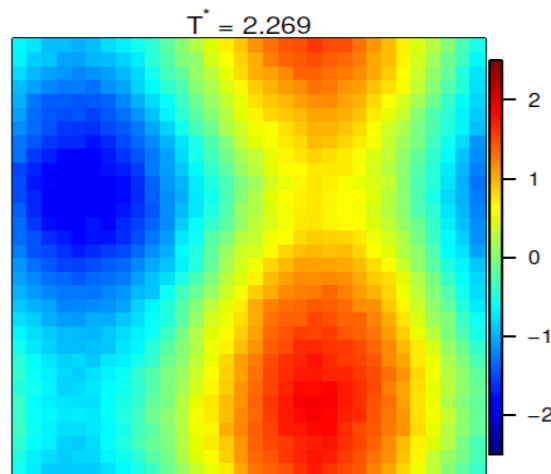
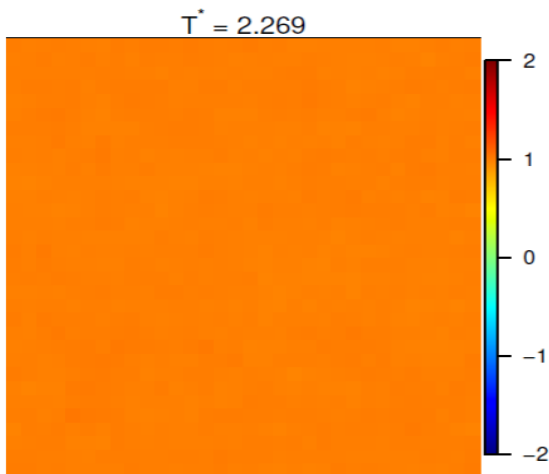
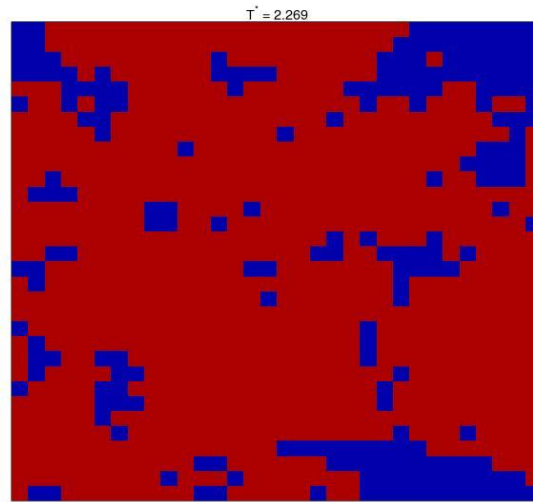
二维Ising模型平衡态本征微观态的权重因子：



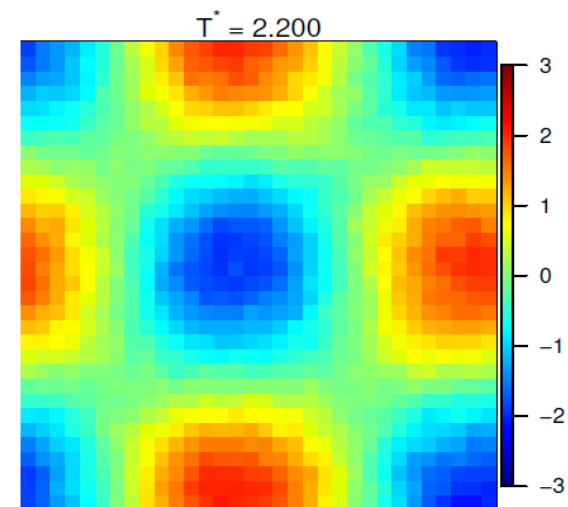
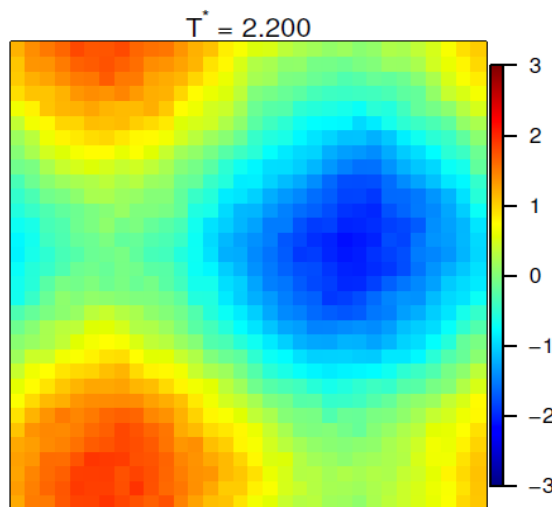
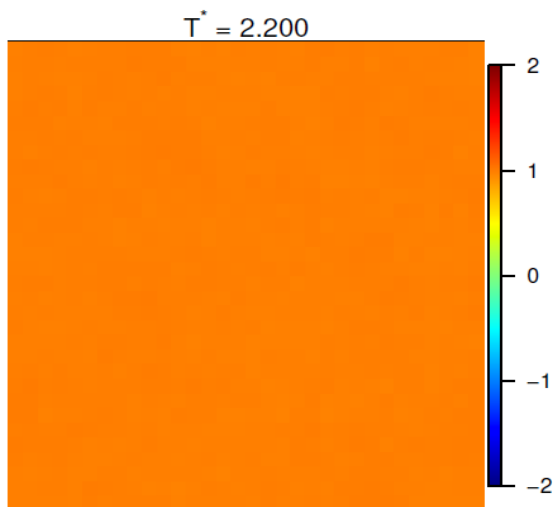
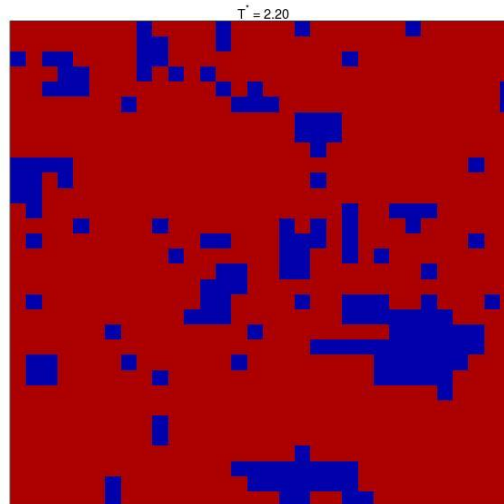
二维Ising模型 ($T \geq T_C$) 的前3大本征微观态:



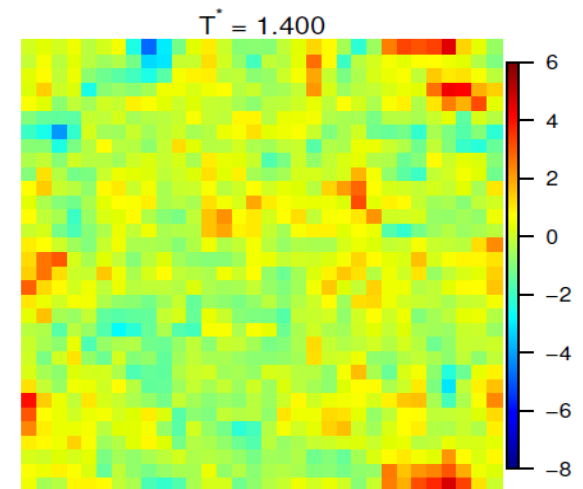
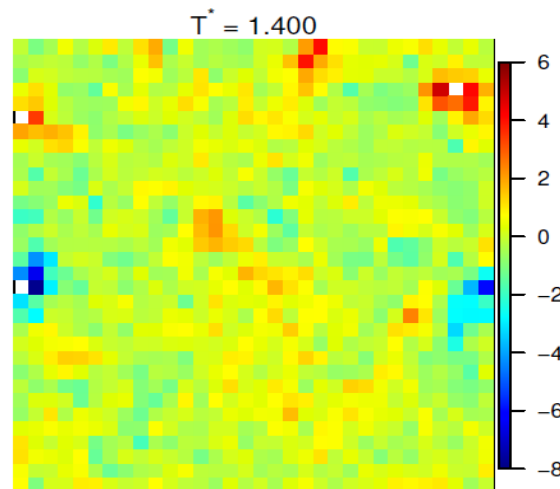
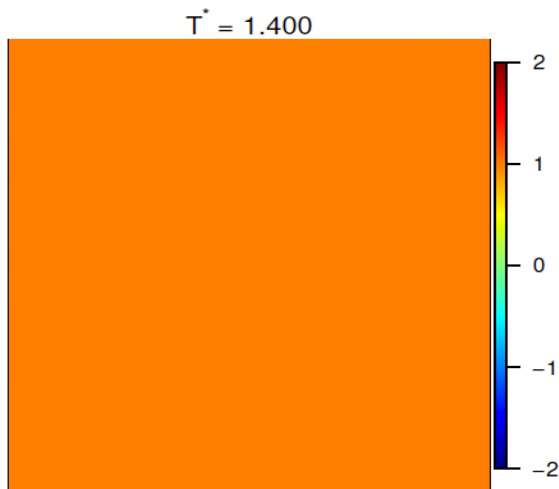
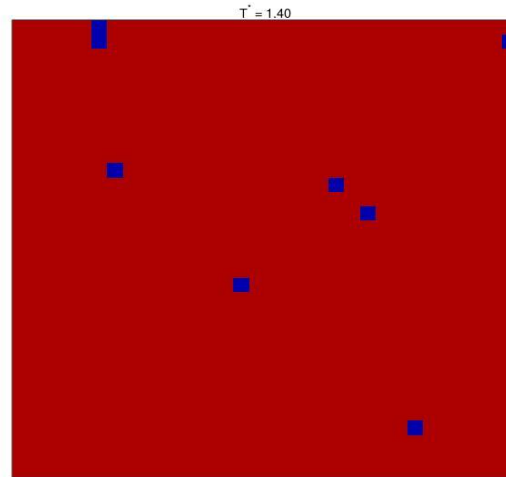
二维Ising模型 ($T \geq T_C$) 的前3大本征微观态:



二维Ising模型 ($T < T_c$) 的前3大本征微观态:



二维Ising模型 ($T < T_c$) 的前3大本征微观态:



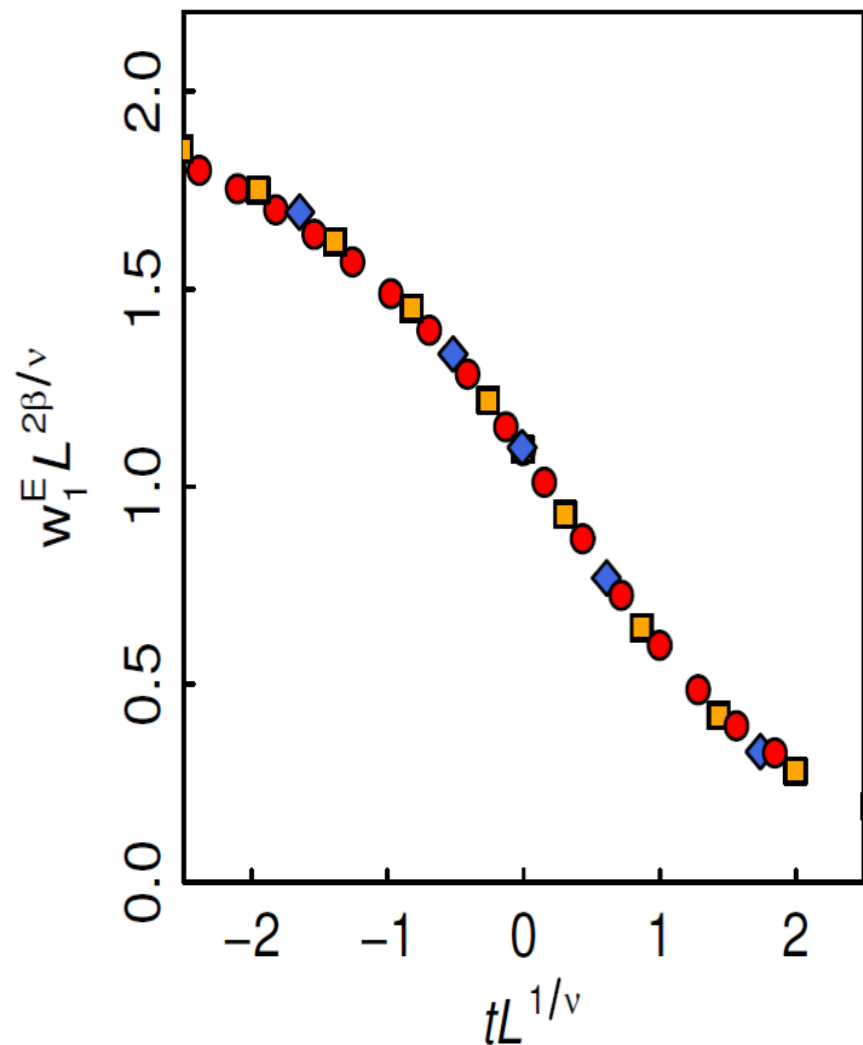
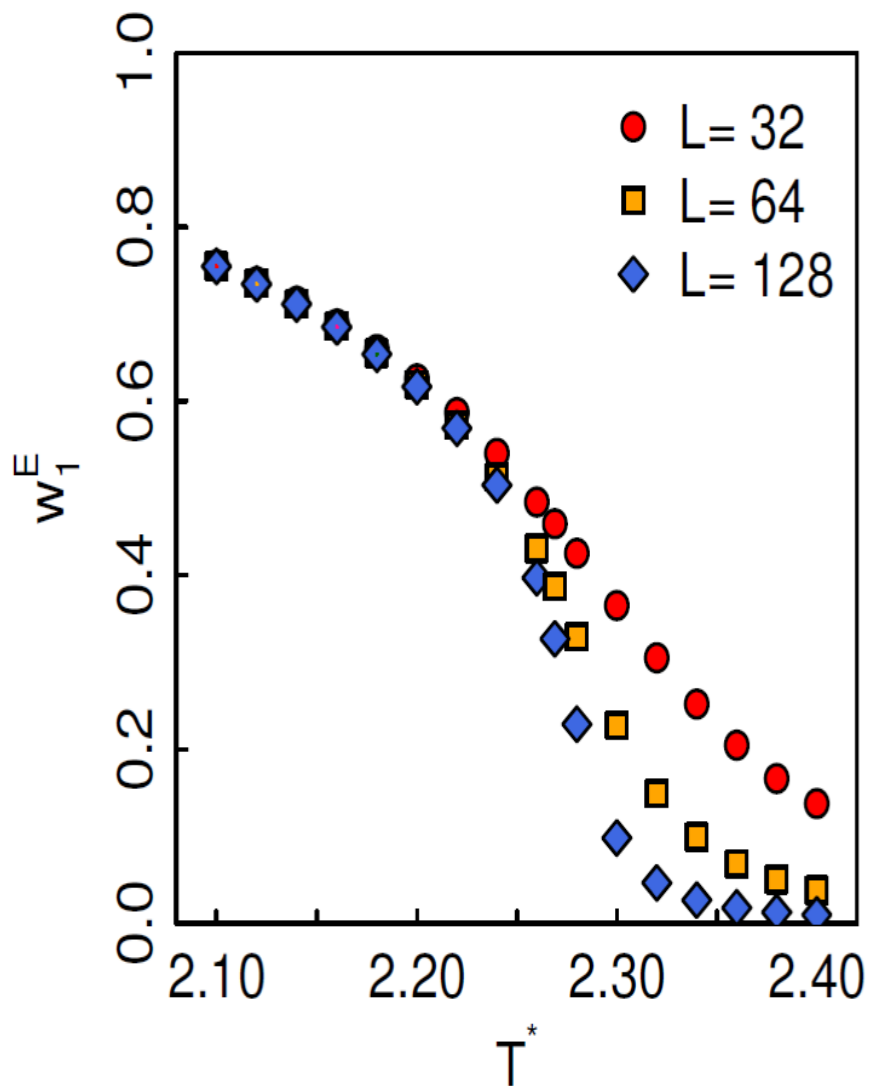
本征微观态权重因子的有限尺度标度性：

$$w_I^E(t, L) = L^{-2\beta/\nu} F_w^I(tL^{1/\nu})$$

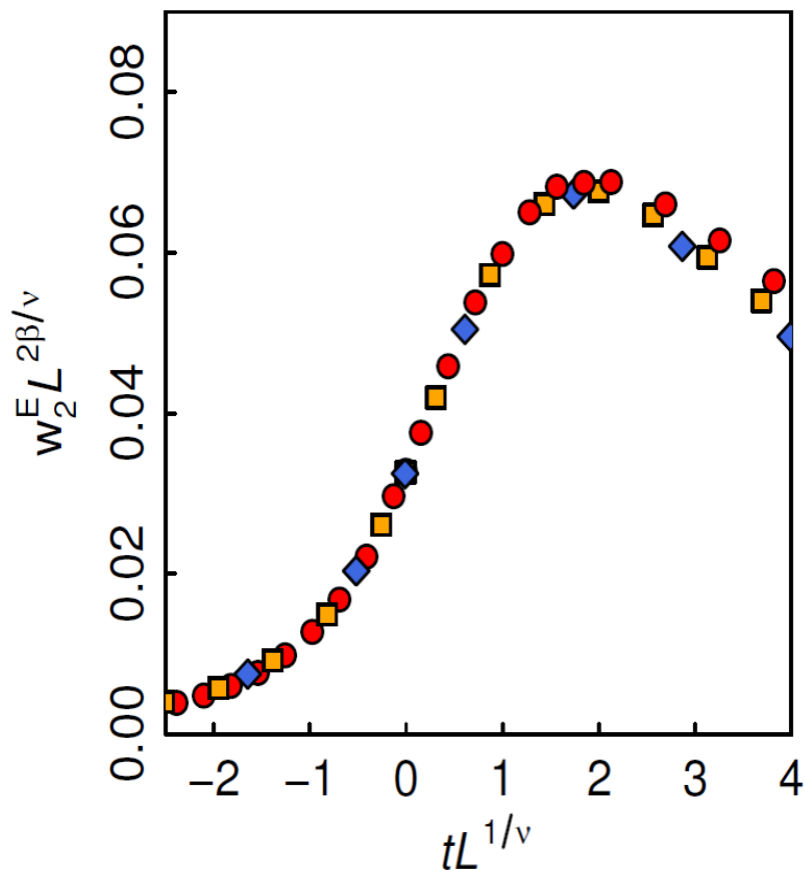
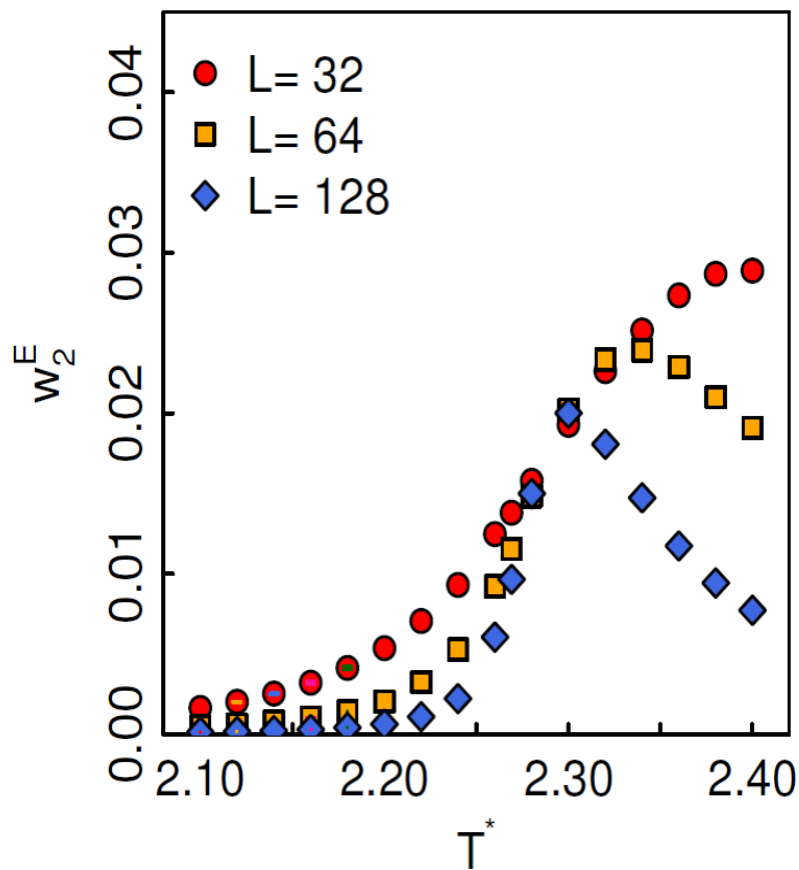
与序参量有限尺度标度性的比较：

$$\langle m \rangle(t, L) = L^{-\beta/\nu} f_m(tL^{1/\nu})$$

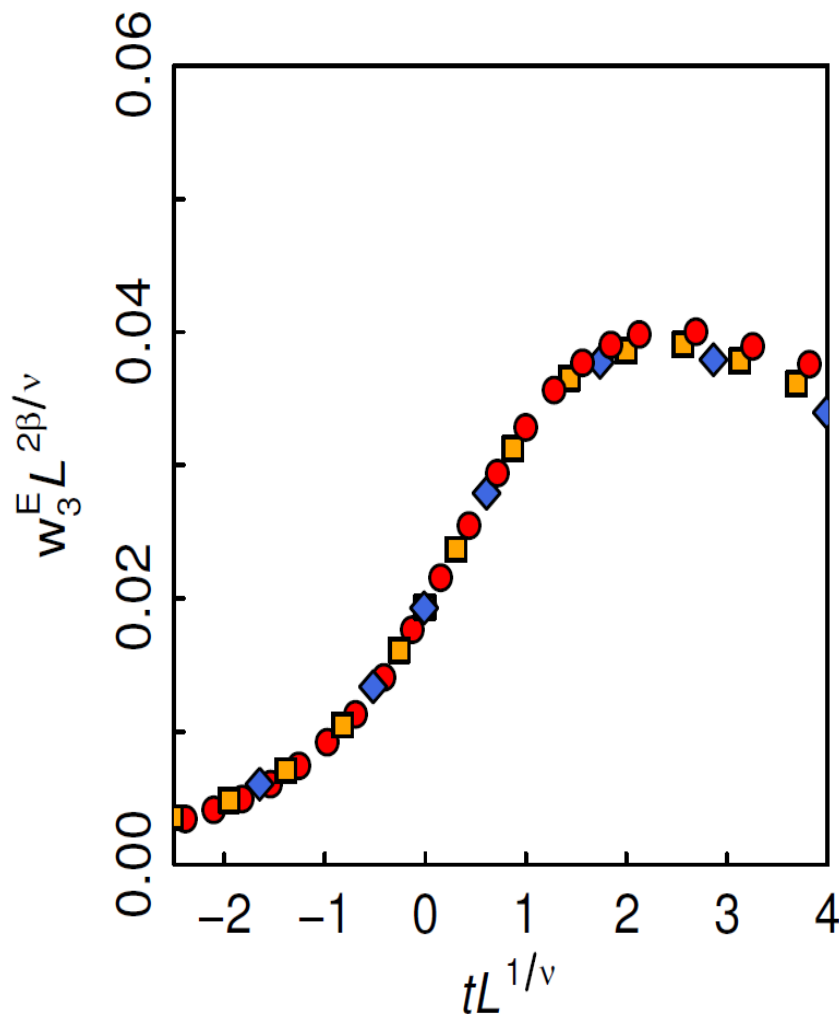
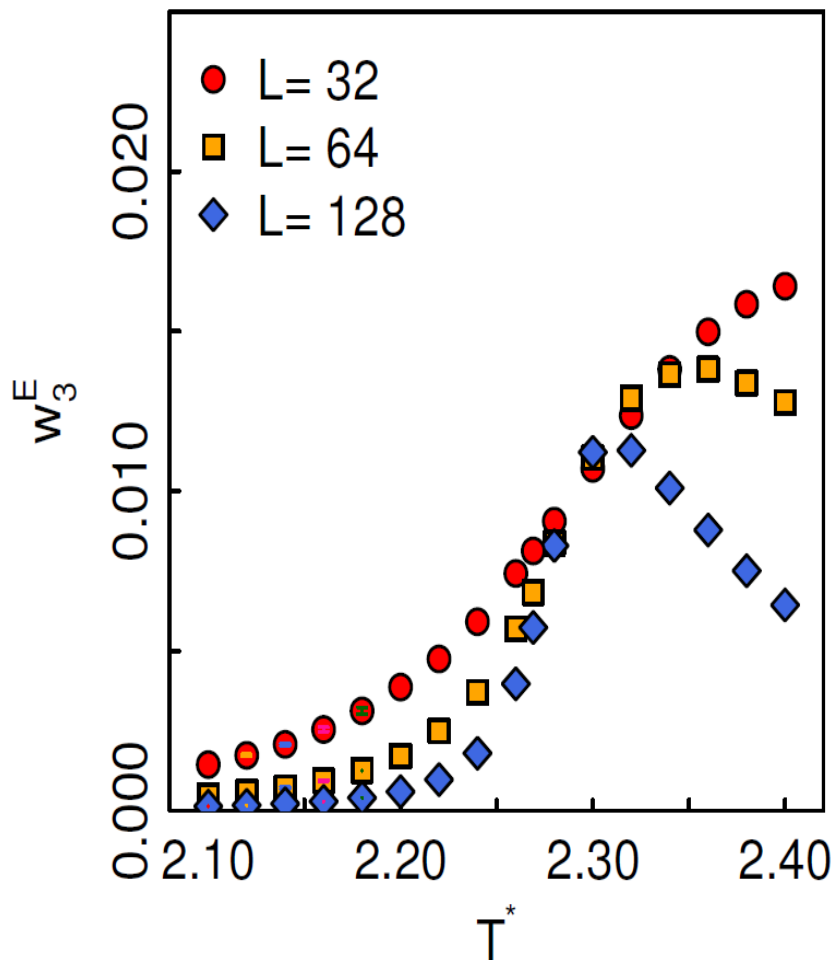
二维Ising模型本征微观态权重因子的有限尺度标度:



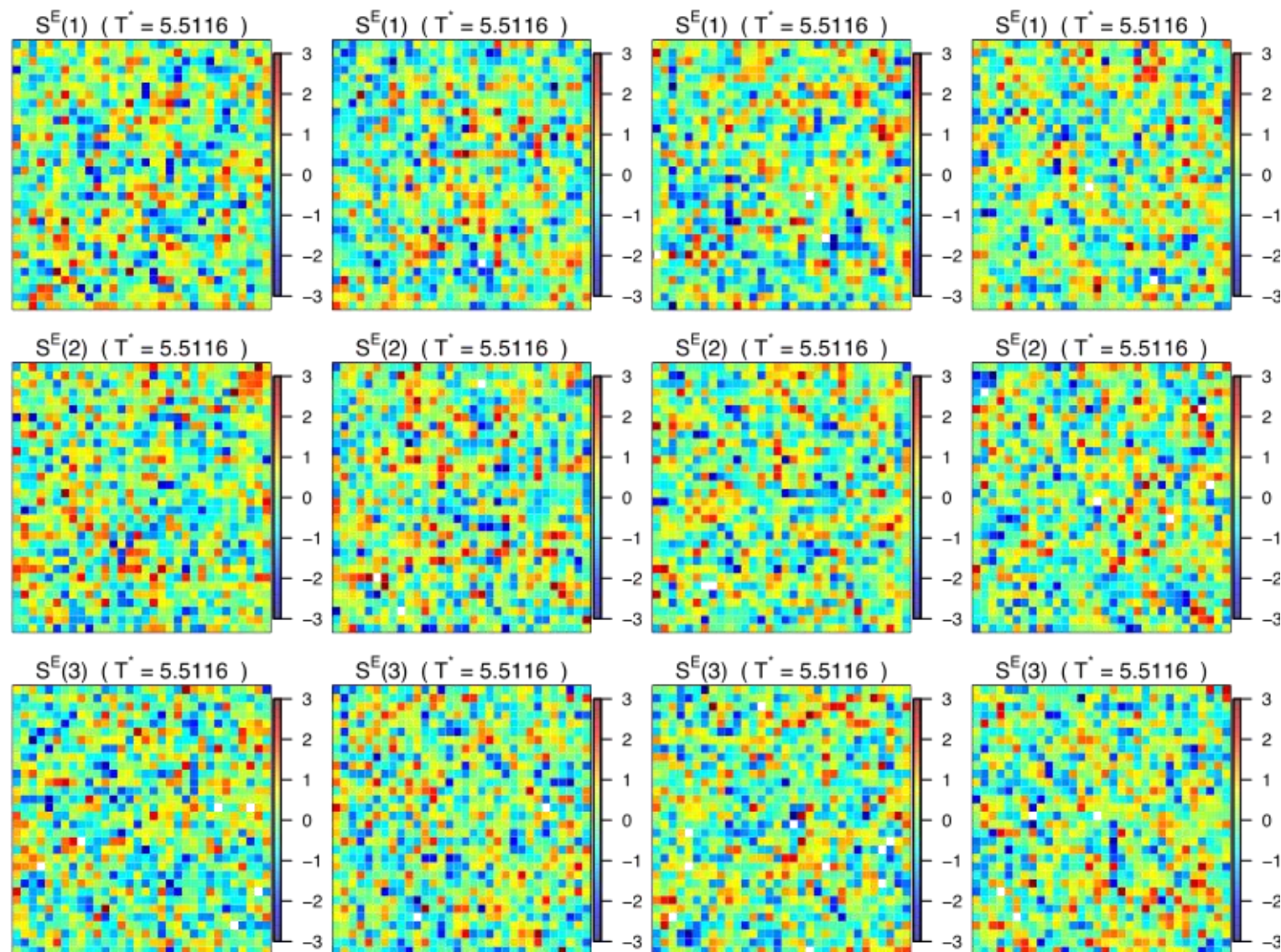
二维Ising模型本征微观态权重因子的有限尺度标度:



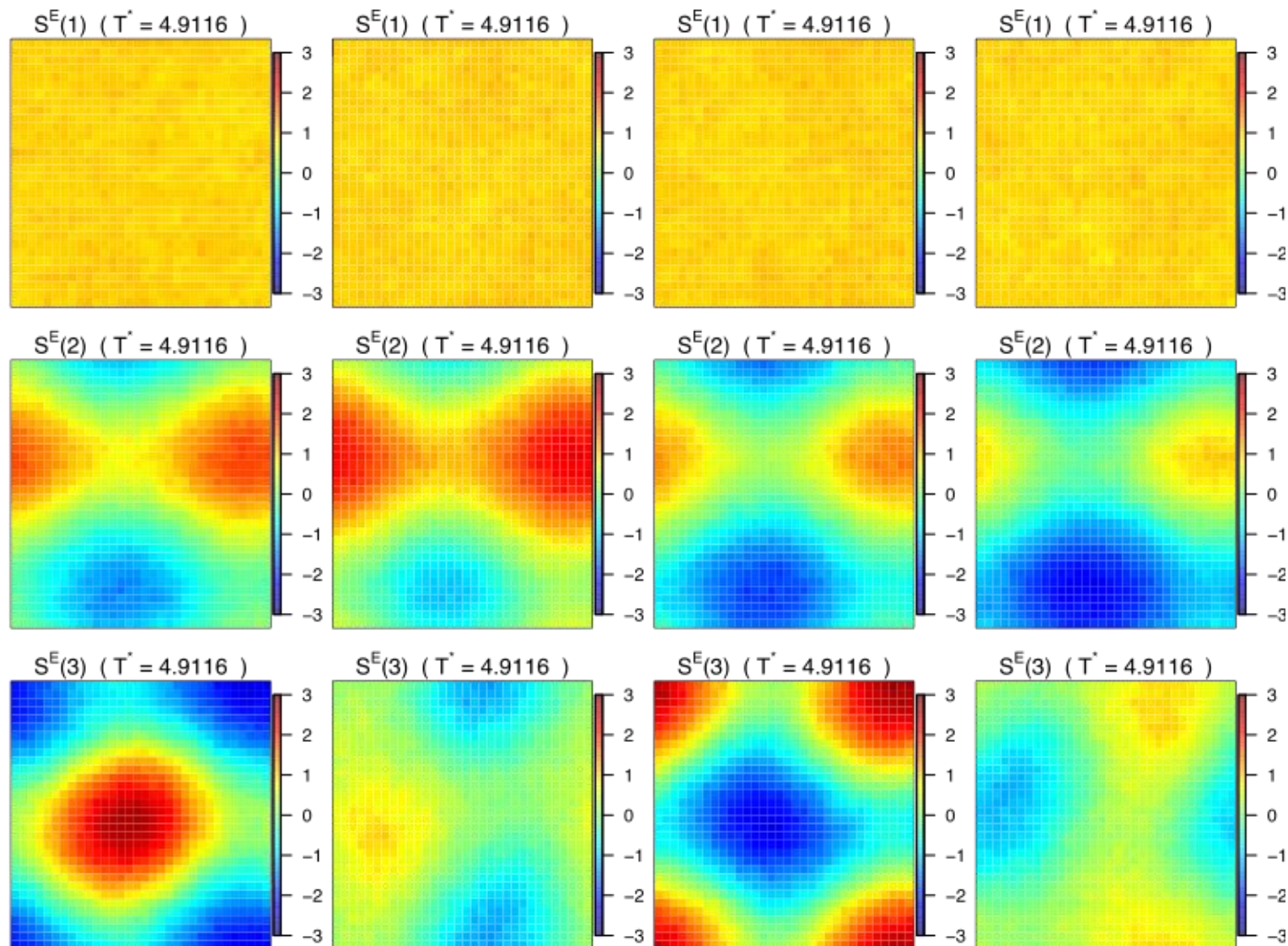
二维Ising模型本征微观态权重因子的有限尺度标度:



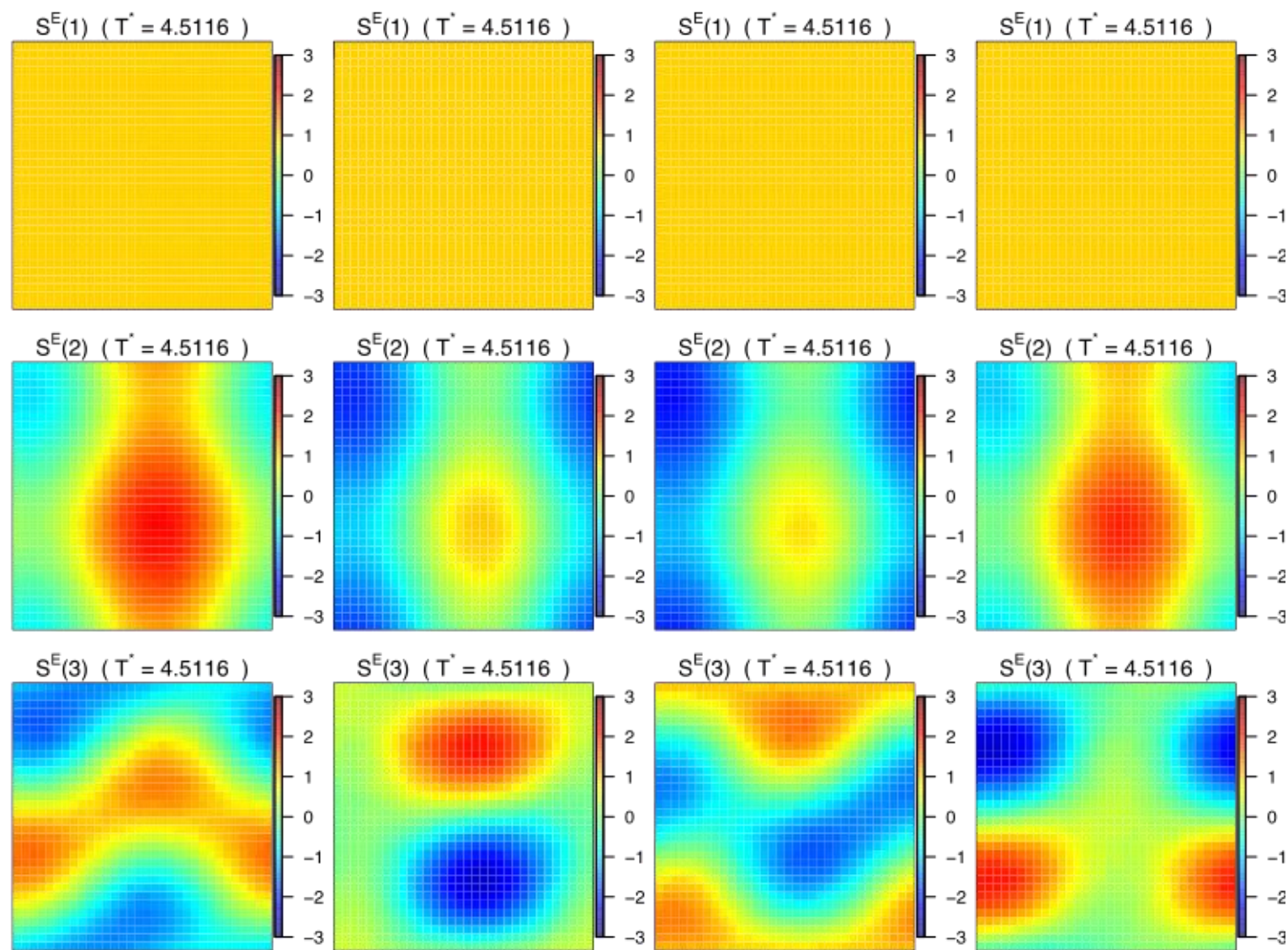
三维Ising模型的本征微观态：



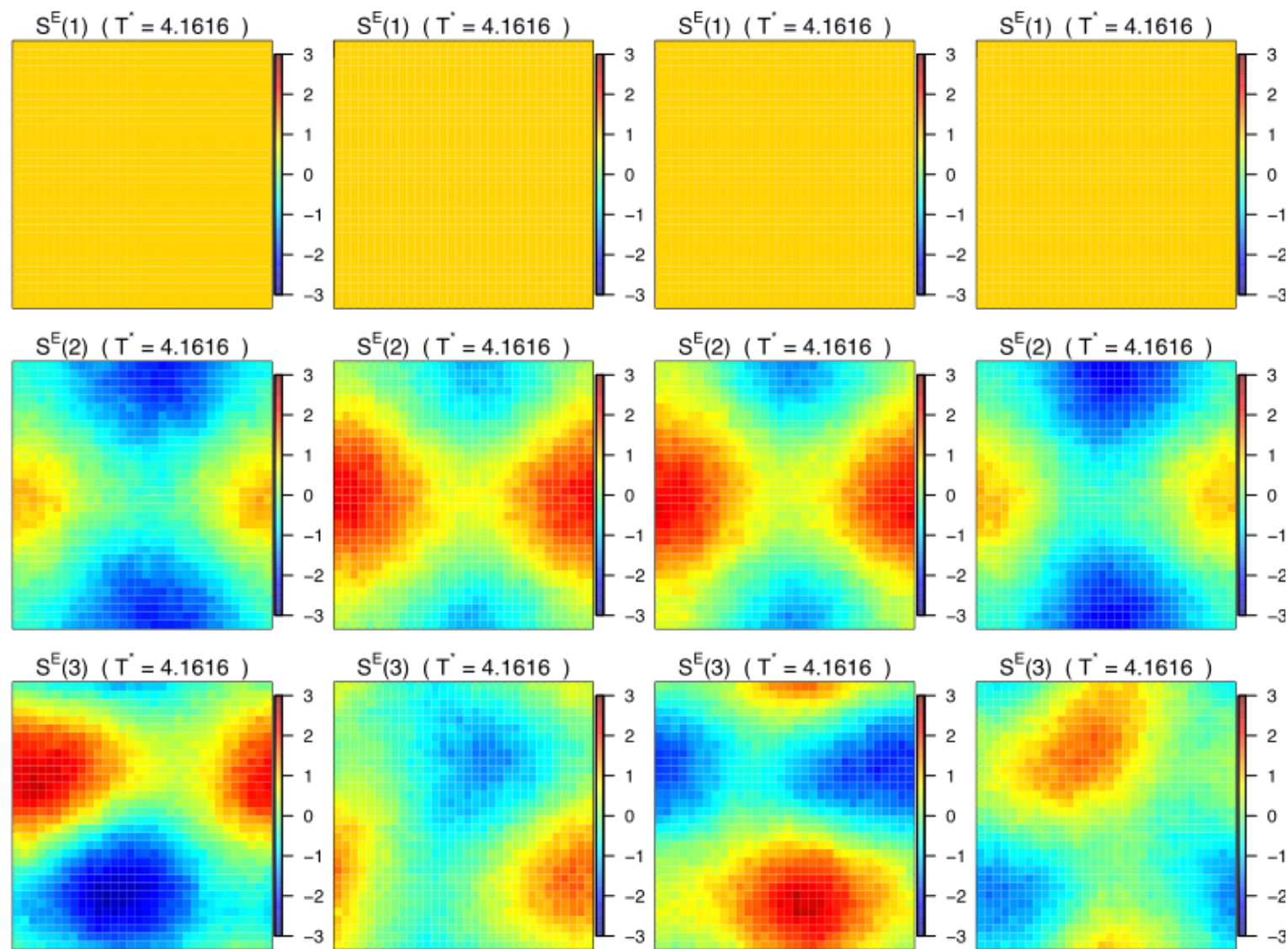
三维Ising模型的本征微观态：



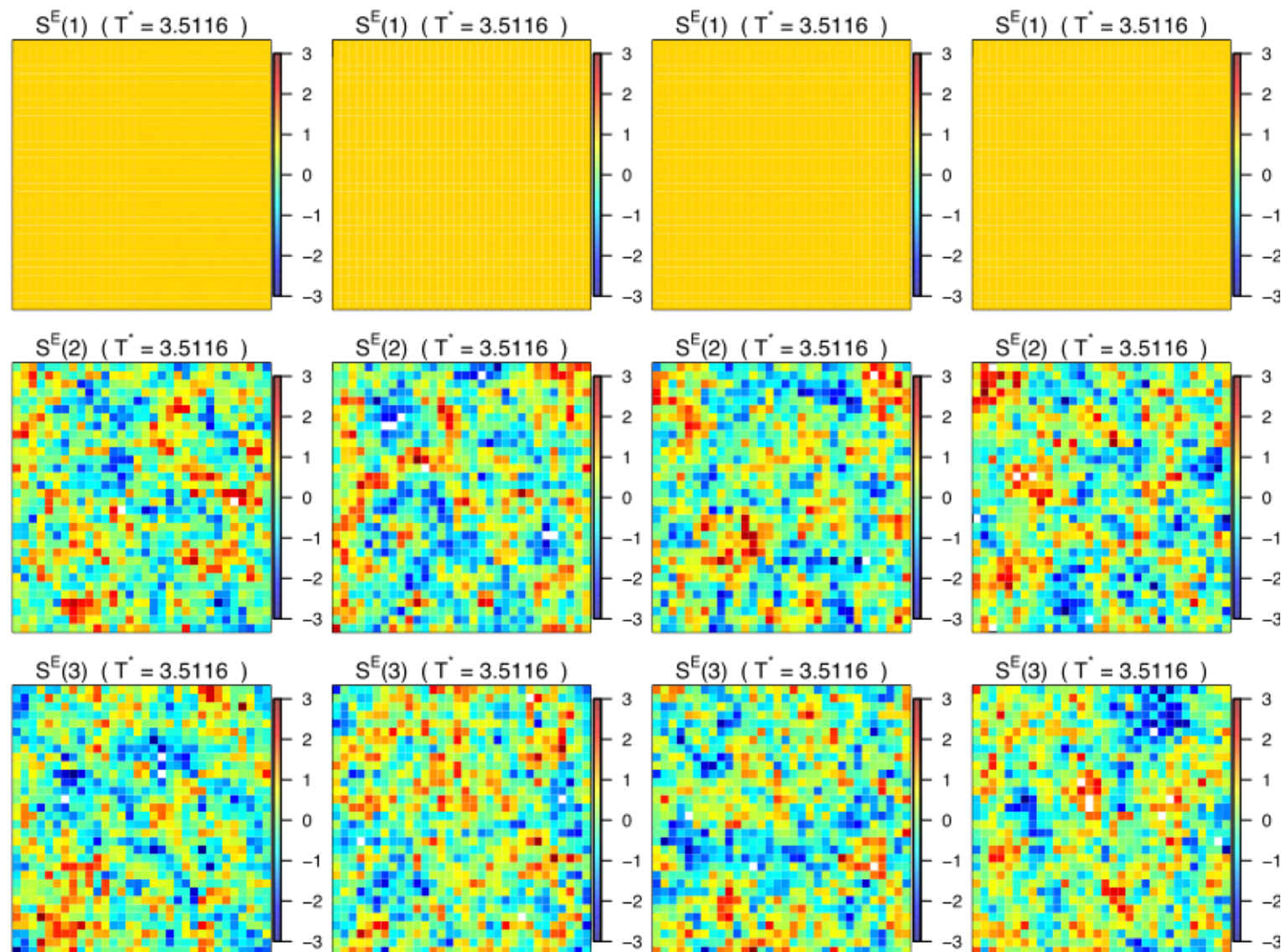
三维Ising模型的本征微观态：



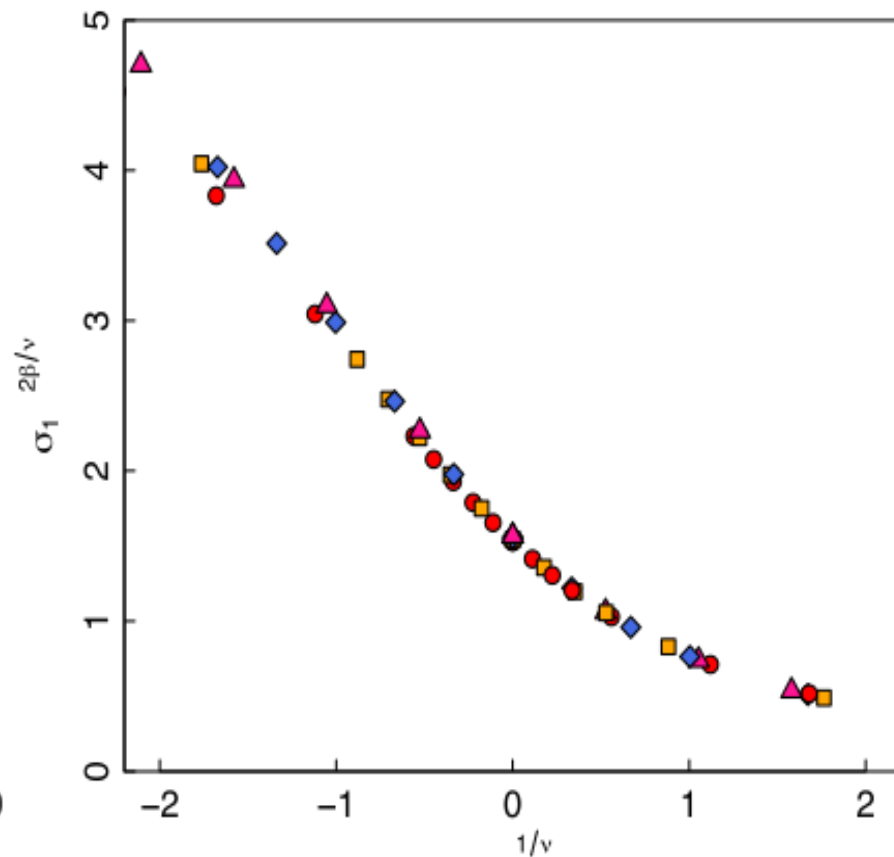
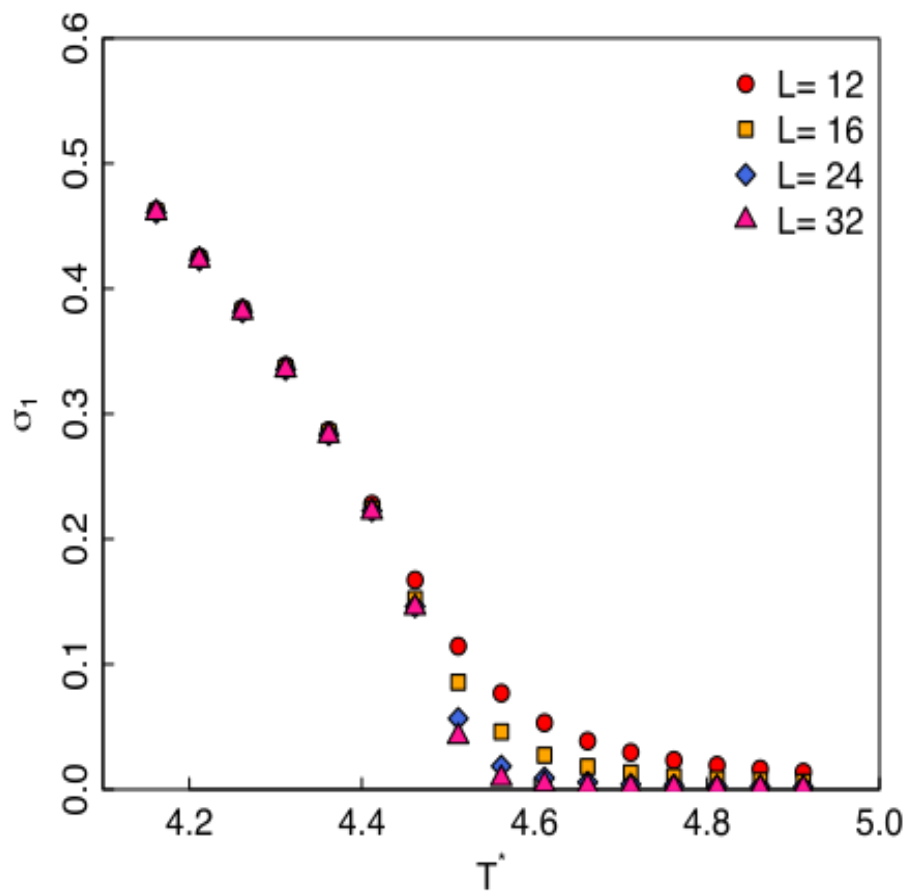
三维Ising模型的本征微观态：



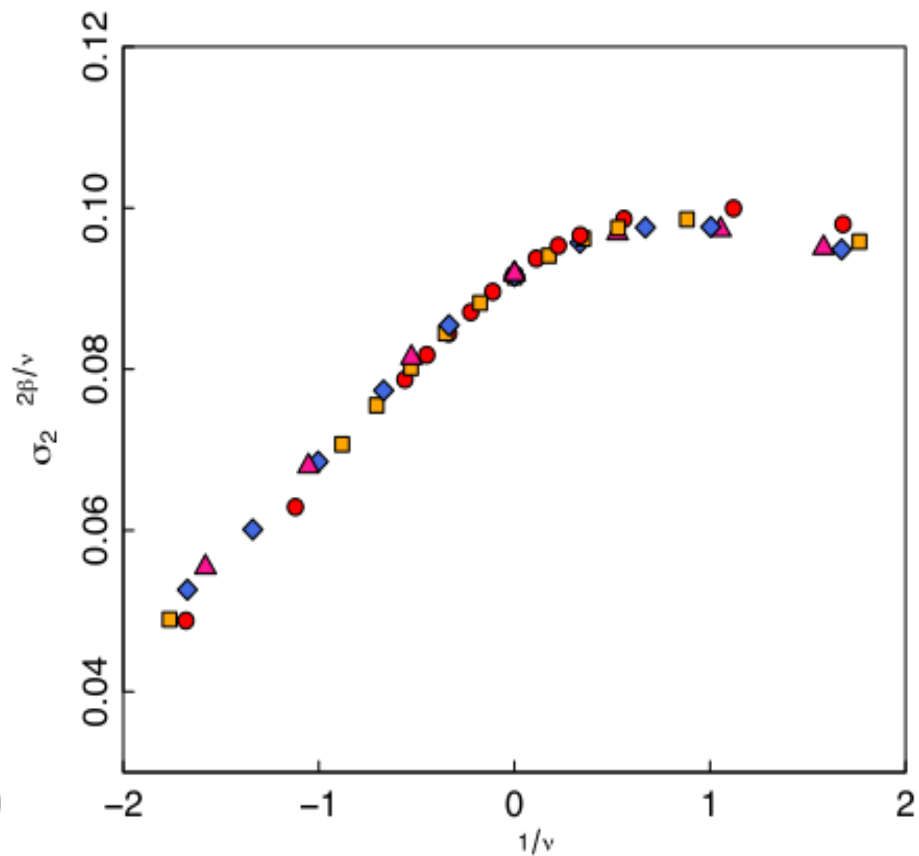
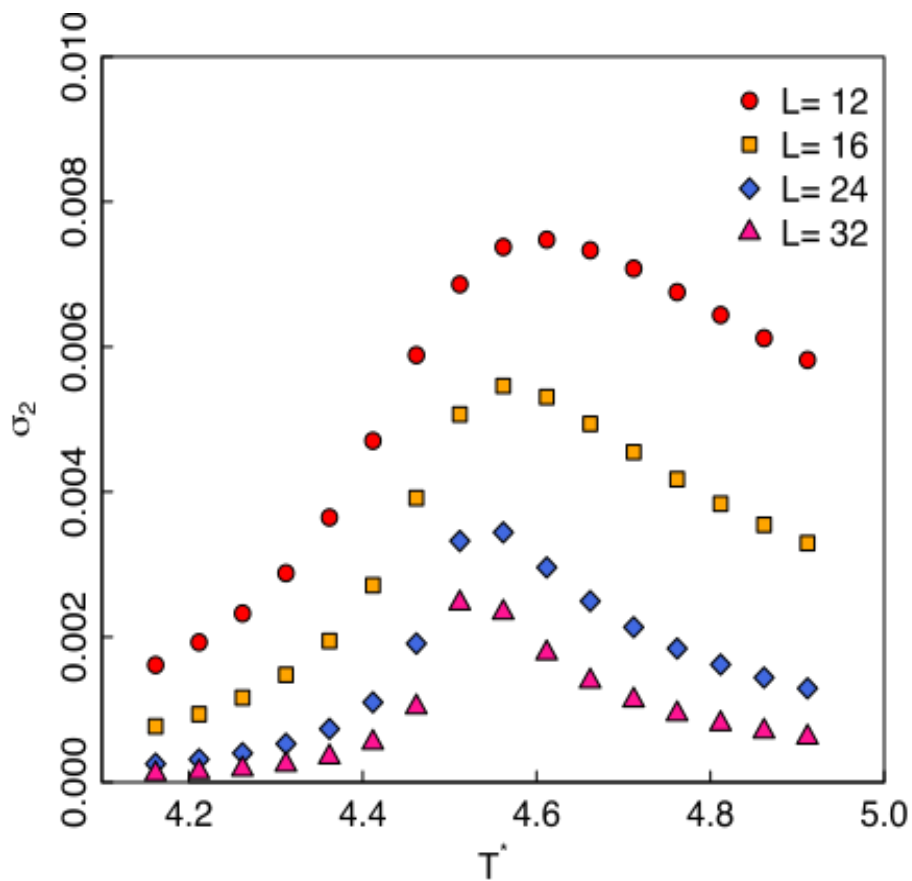
三维Ising模型的本征微观态：



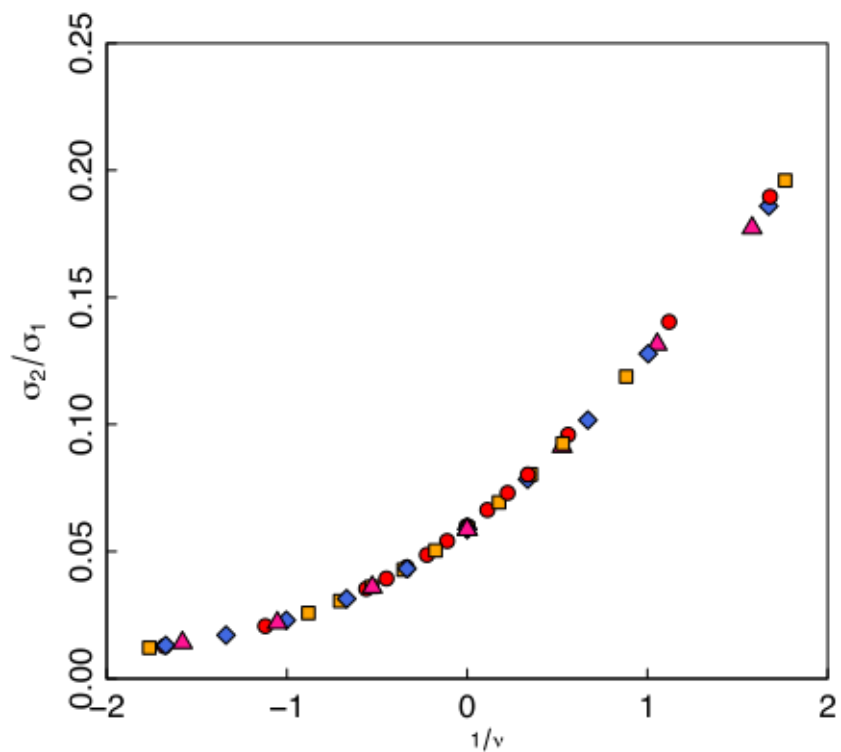
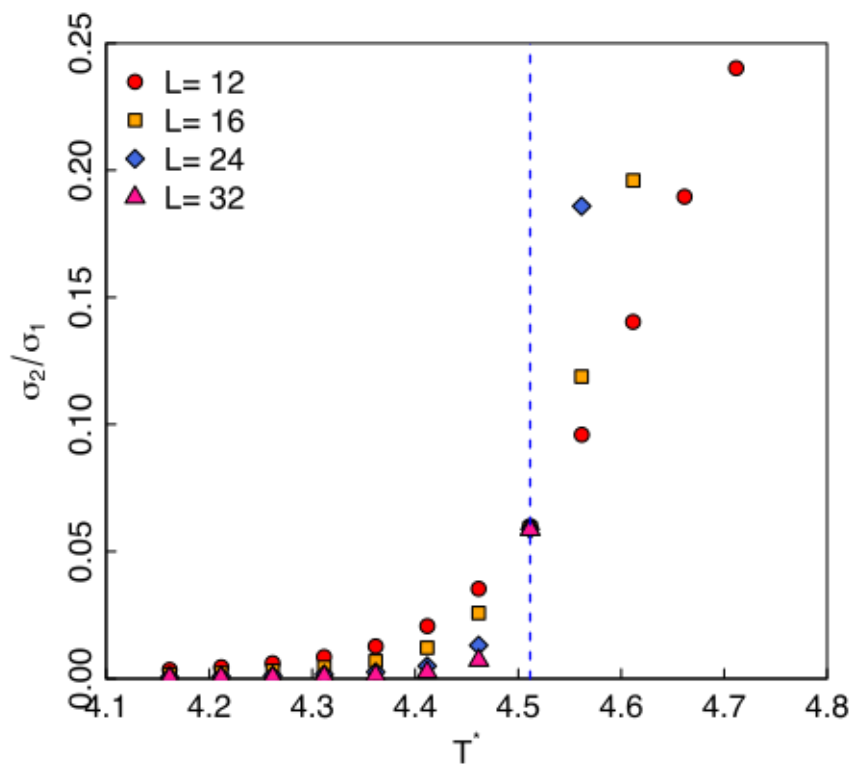
三维Ising模型最大本征值的有限尺度标度性：



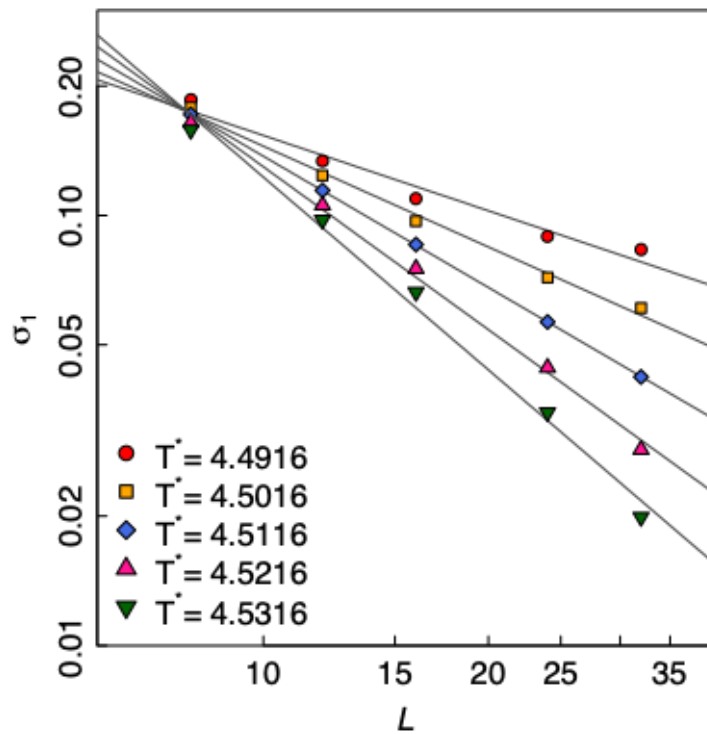
三维 Ising 模型最二本征值的有限尺度标度性:



三维Ising模型最大与第二大本征值的比值：



三维Ising模型最大本征值对尺度的依赖：



全球温度涨落模式分析：

At a time t , the surface temperature of a grid i is $T_i(t)$. Its average during a period M can be calculated as

$$\langle T_i \rangle = \frac{1}{M} \sum_{t=1}^M T_i(t) . \quad (25)$$

The grid i has temperature fluctuations $\delta T_i(t) = T_i(t) - \langle T_i \rangle$. It is more proper for us to consider the normalized fluctuations

$$S_i(t) = \delta T_i(t) / \Delta_i , \quad (26)$$

where $\Delta_i = \sqrt{\frac{1}{M} \sum_{t=1}^M (\delta T_i(t))^2}$.

全球温度观测数据:

Our study is based on daily surface air temperature (2 m) provided by the National Centers for Environmental Prediction-National Center for Atmospheric Research (NCEP-NCAR) Analysis[12]. The dataset spans the time period between 1950-01-01 and 2018-12-31. The Oceanic Niño Index (ONI) is used to define El Niño and La Niña events by the National Oceanic and Atmospheric Administration (NOAA). The ONI is defined as 3 month running mean of ERSST.v5 SST anomalies in the Niño 3.4 region (5°S - 5°N , 190°E - 240°E).

Using the dataset spanning from 1950-01-01 to 2018-12-31, we can get an $N \times M$ ensemble matrix \mathbf{A} with elements

$$A_{it} = \delta S_i(t) . \quad (40)$$

本征微观态随时间演化的谱分析:

$$V_I(t) = \sum_{n=0}^{M-1} a_n^I e^{i\frac{2\pi}{M}nt} \quad (41)$$

where

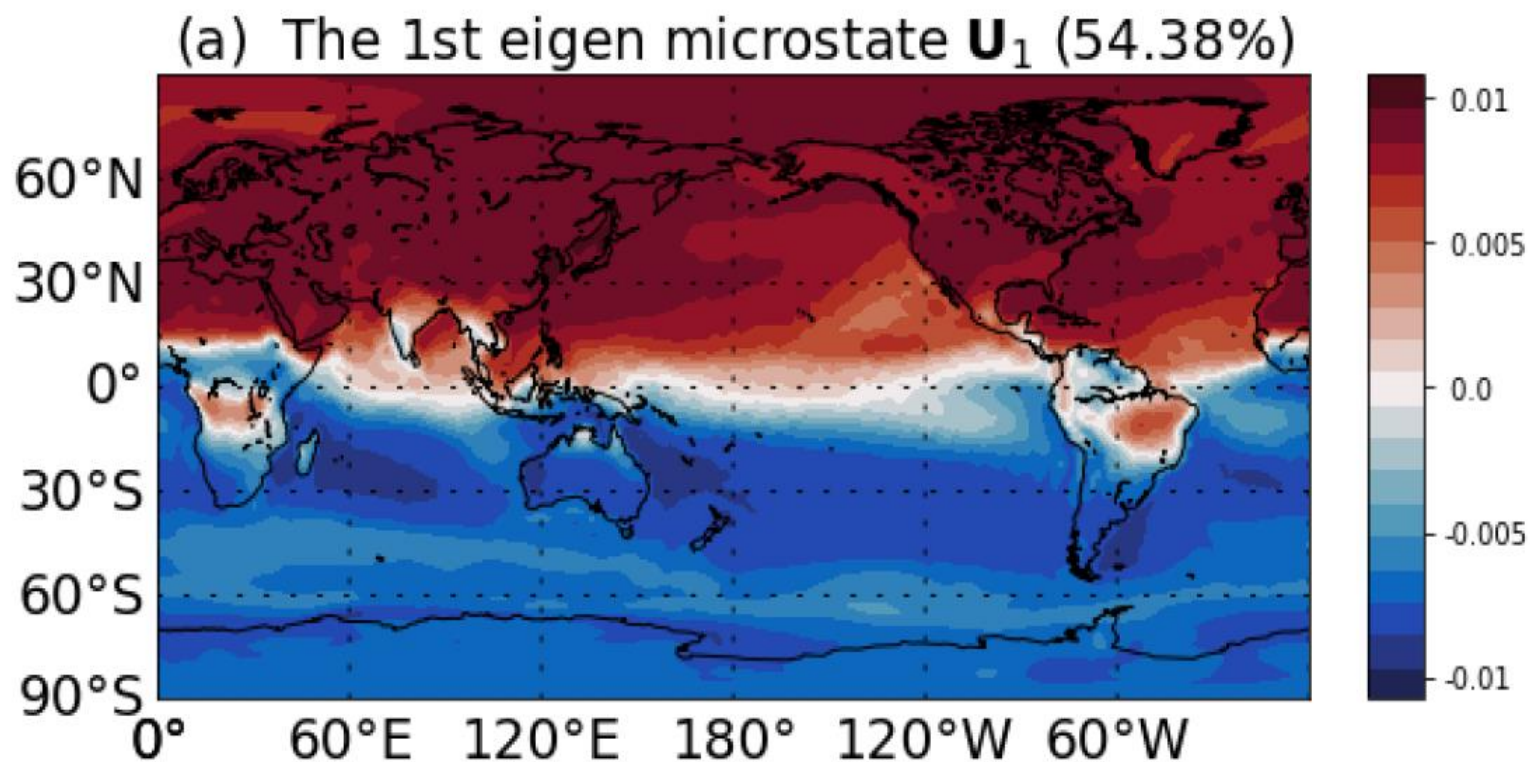
$$a_n^I = \frac{1}{M} \sum_{t=0}^{M-1} V_I(t) e^{-i\frac{2\pi}{M}nt} . \quad (42)$$

In Fig.12, the Fourier power spectrum density

$$I_n = \frac{|a_n^I|^2}{\sum_{n=0}^{M-1} |a_n^I|^2}$$

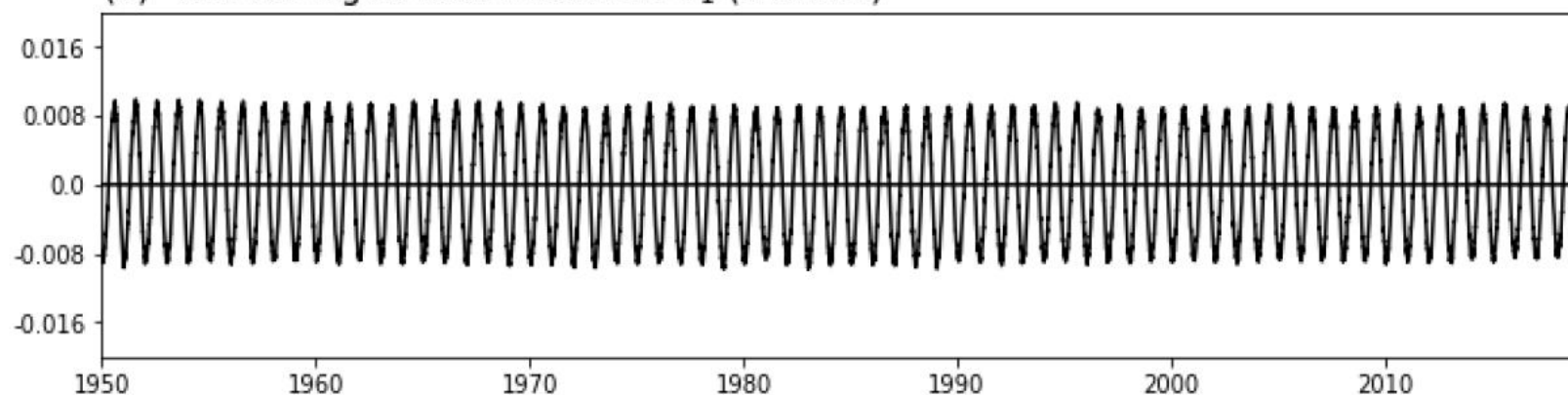
are plotted with respect to its period $T_n \equiv M/n$.

第一大本征微观态 (1950-01-01至2018.12-31)

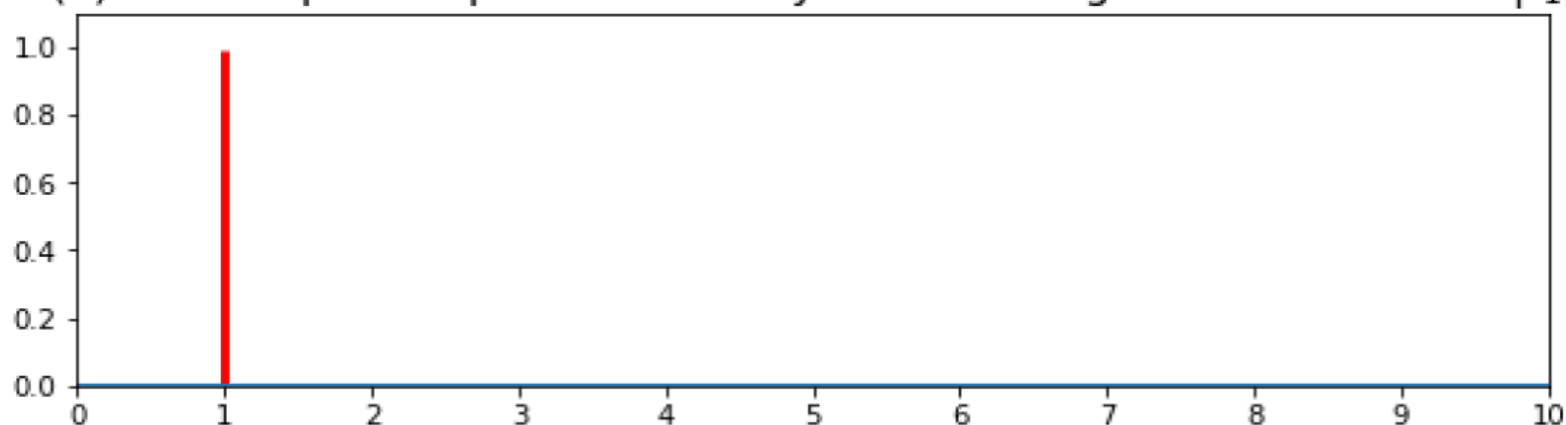


第一大本征微观态

(a) The 1st eigen time evolution \mathbf{V}_1 (54.38%)



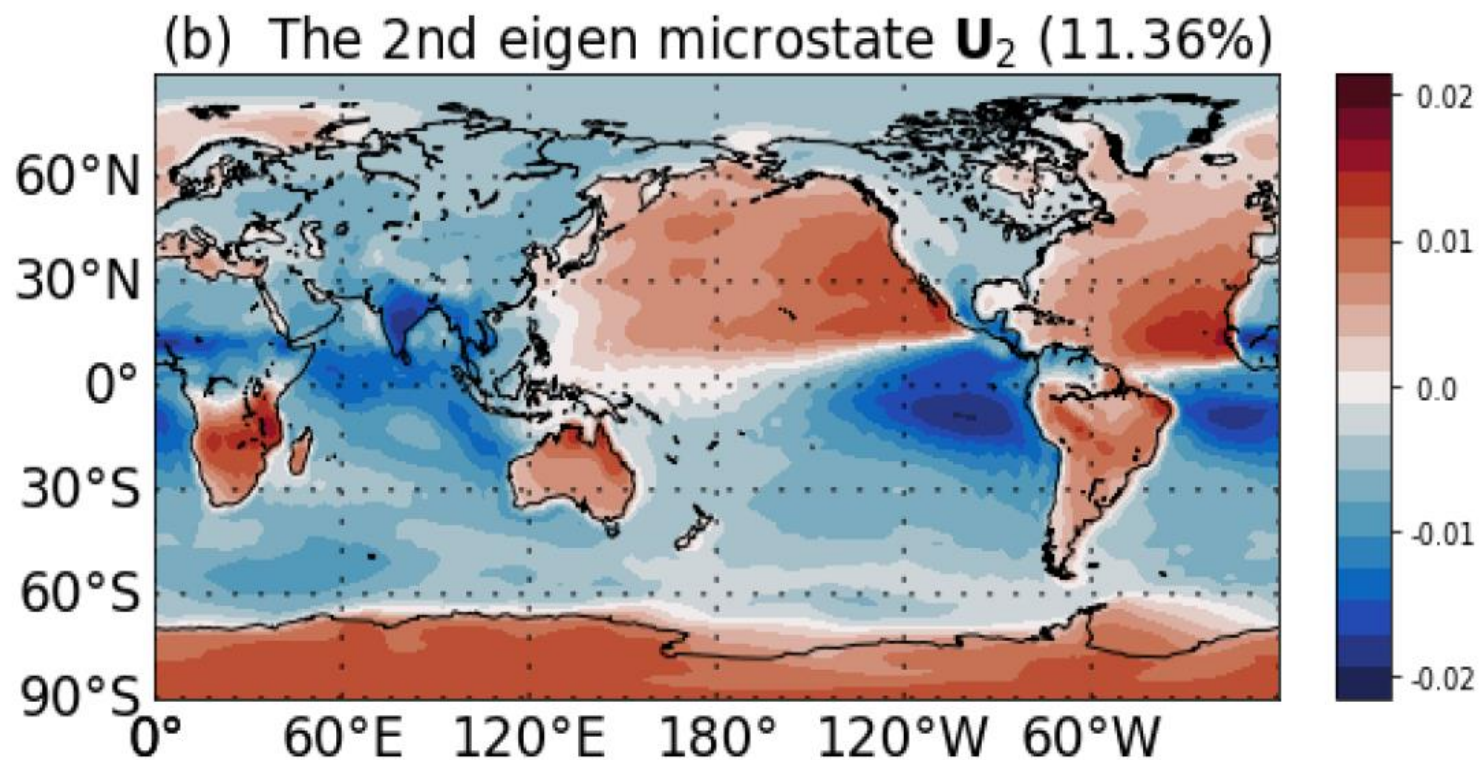
(a) Fourier power spectrum density of the 1st eigen time evolution $|\mathbf{V}_1|$



第一大本征微观态:

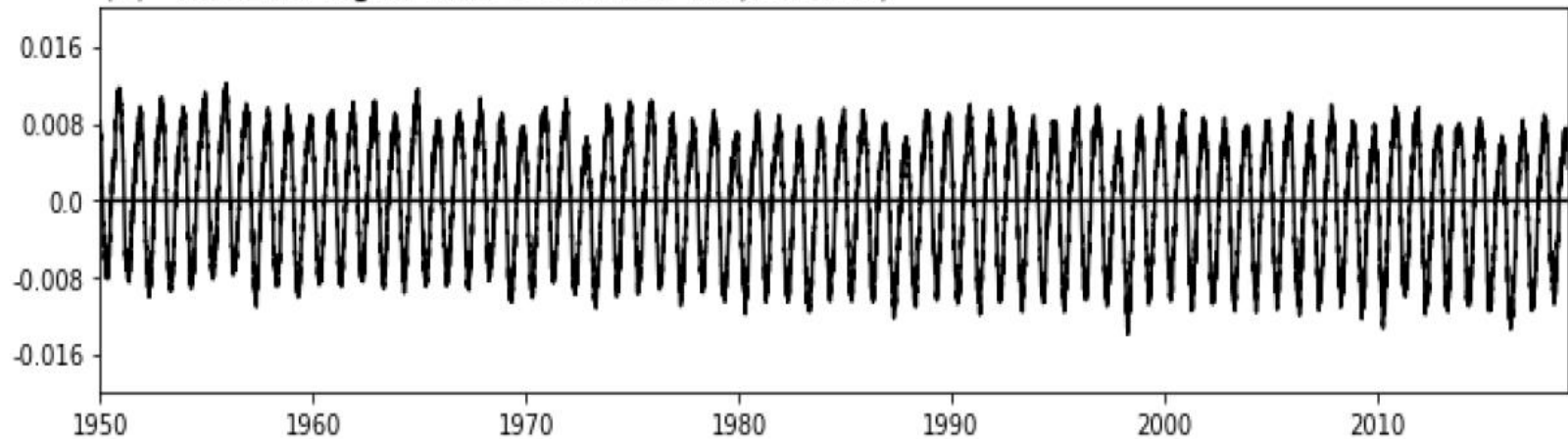
As presented in Fig. 10(a), the first Eigen Microstate (EM1) reveals a classic solstitial mode, explaining 54.38% of the total variance. Its spatial pattern exhibits an inter-hemisphere contrast. This asymmetry is roughly a mirror image along the equator, although the slight shift is evident over the African, South American and Eastern Pacific sections. The spectrum analysis (Fig. 12(a)) of the corresponding time series (Fig. 11(a)) shows a robust peak of 1 year, following the annual variation of the solar zenith angle. Further results (Fig. 14) show that the maximum of EM1 often occurs in August and the minimum of EM1 occurs in Late January, implying the 1 month delay of air temperature after the solar forcing.

第二大本征微观态（海陆温差）

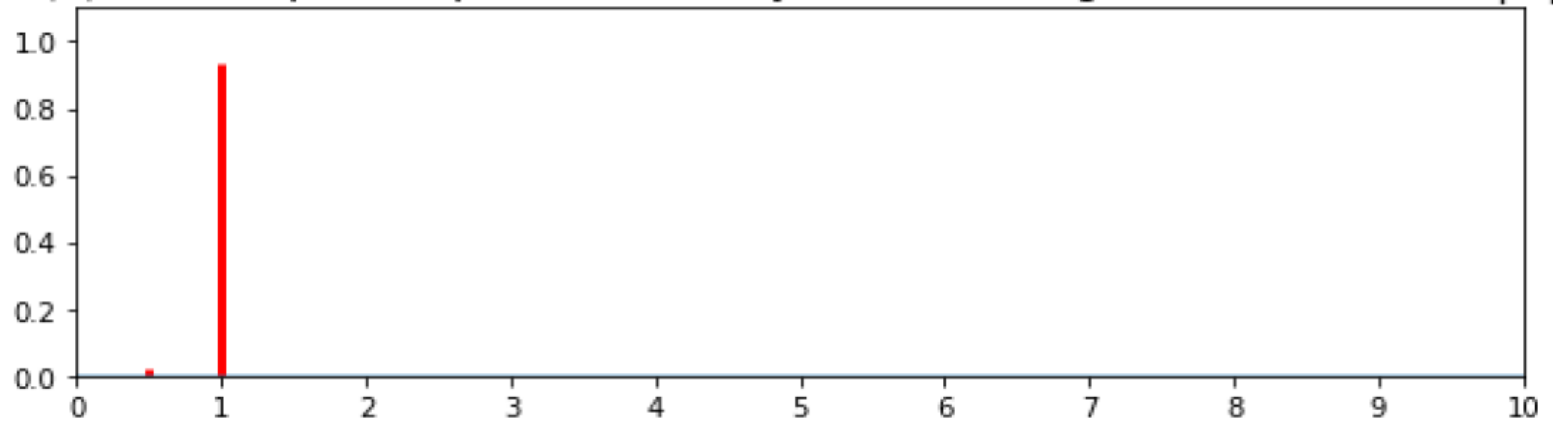


第二大本征微观态

(b) The 2nd eigen time evolution \mathbf{V}_2 (11.36%)



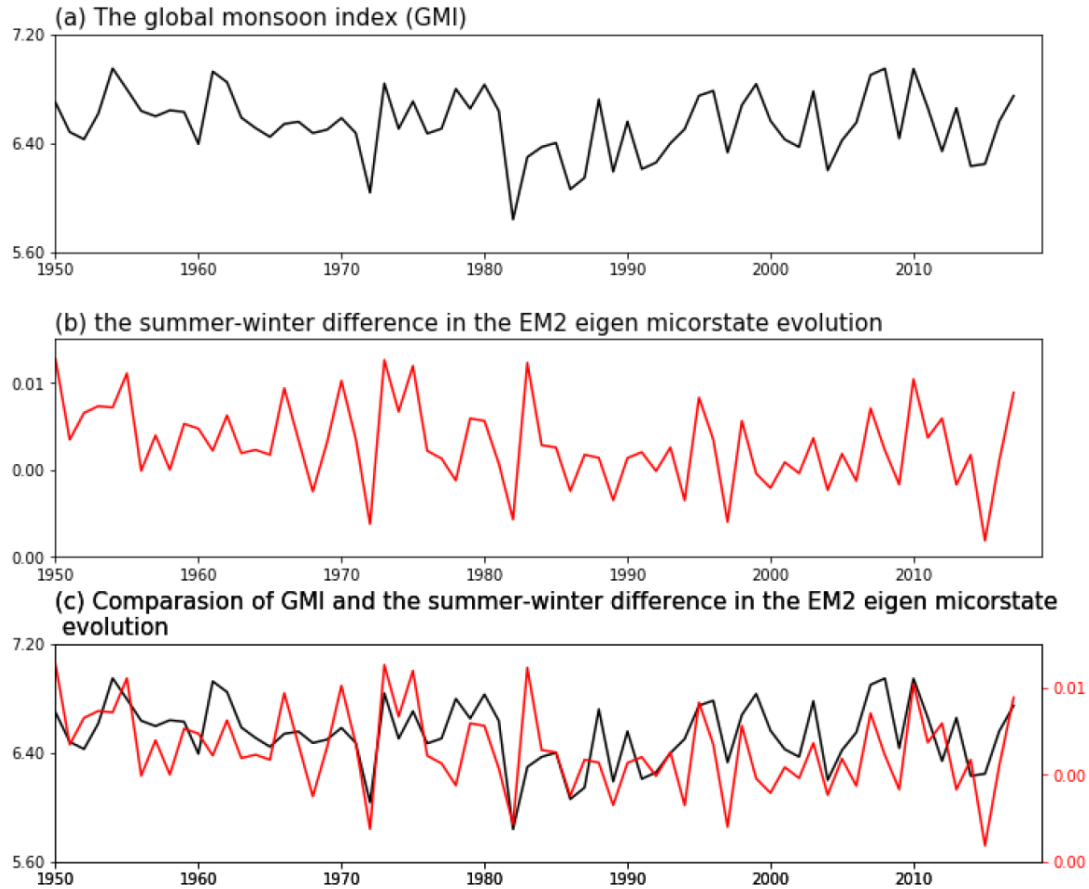
(b) Fourier power spectrum density of the 2nd eigen time evolution $|\mathbf{I}_2|$



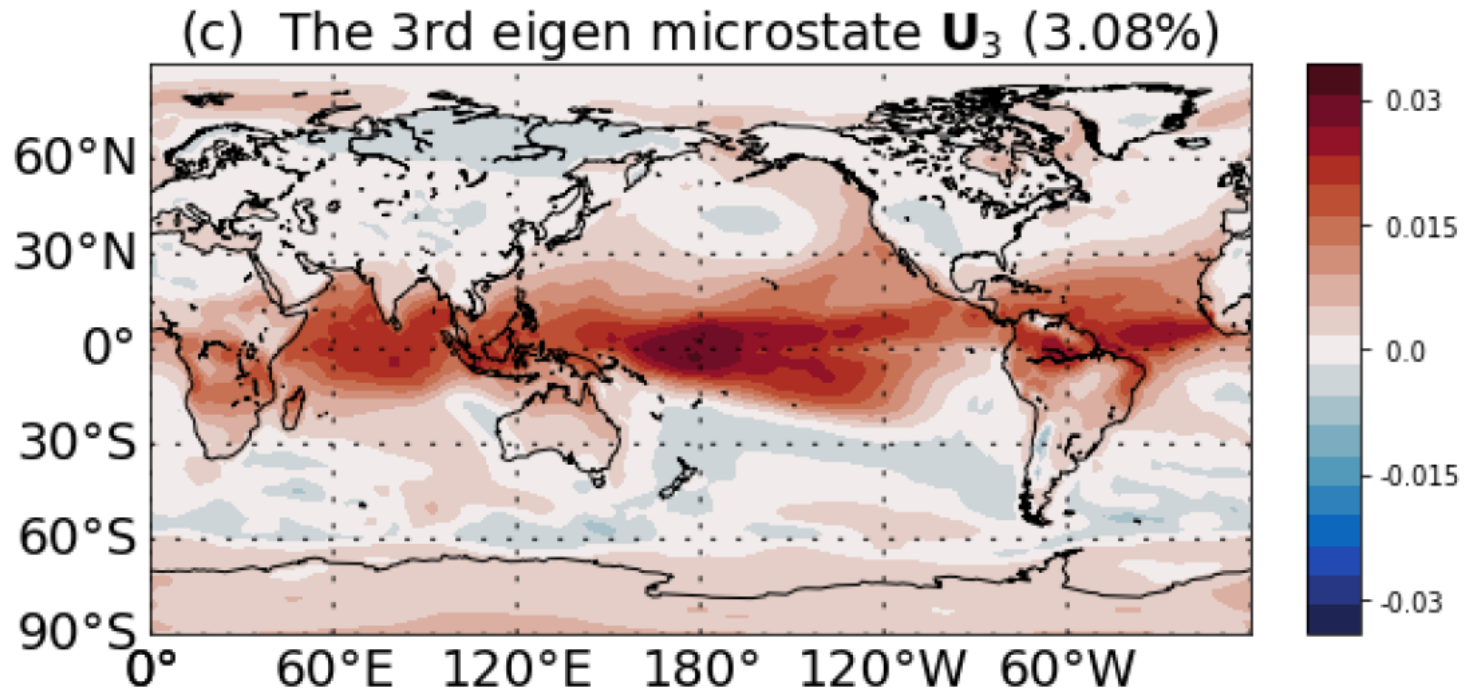
第二大本征微观态对应海陆温差、是季风的推手

variation of this mode. A remarkable land-sea contrast is observed in EM2. In the southern (northern) hemisphere, the surface air temperature warms up (cools down) faster over the continents than that over the oceans due to the land-sea thermal capacity difference. It should be noted that this thermal contrast in the tropical-subtropical regions drives the local monsoons over the South Asia ([14]) Australia [15], West Africa [16], North America[17], and South America[18]. Bin Wang et al.[13] proposed the concept of global monsoon system by considering the seasonal contrast of precipitation globally. It is interesting that the domain with the spatial absolute intensity above 40% of the maximum absolute intensity in EM2 resembles the global monsoon area derived by Wang et al. [13] as is presented in Fig. 15, with the spatial matching degree reaching 70%. (Since the the land-sea thermal contrast is not the only cause of East Asia monsoon, the monsoon area near East Asia is not very matched.[19]) We further compare the summer-winter difference in the EM2 eigen microrstate evolution with the global monsoon index (Fig. 16). Again, a significant correlation 0.52 is obtained. The above evidences reveal that EM2 represents the land-sea contrasts of SAT which is primary driver for monsoon.

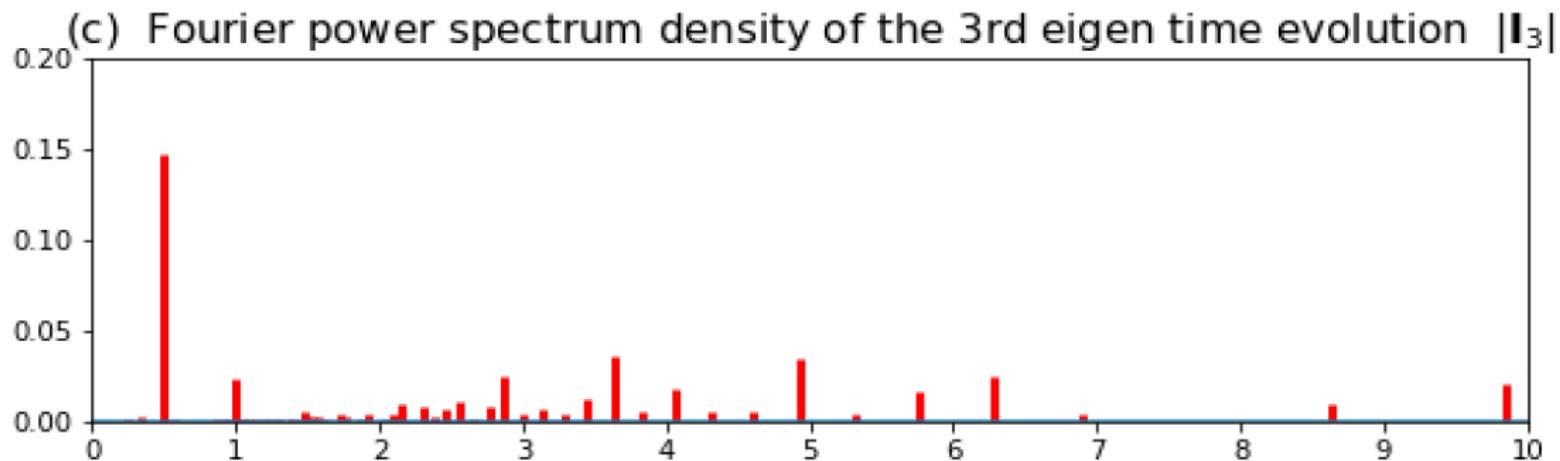
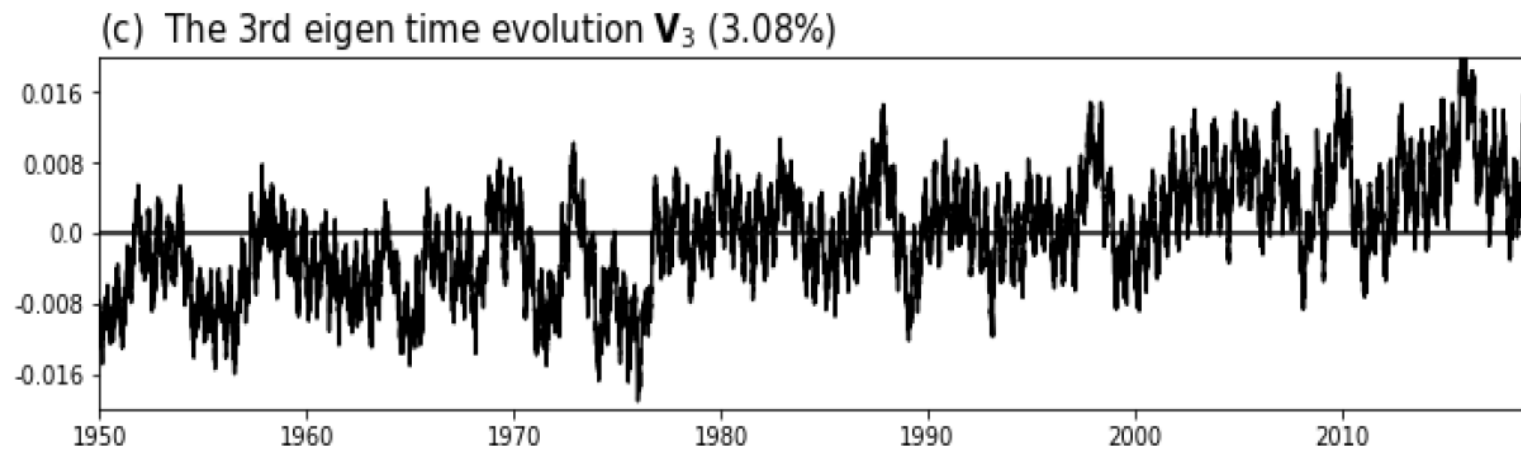
与全球季风指数的比较:



第三大本征微观态 (**Hadley cell**)



第三大本征微观态:

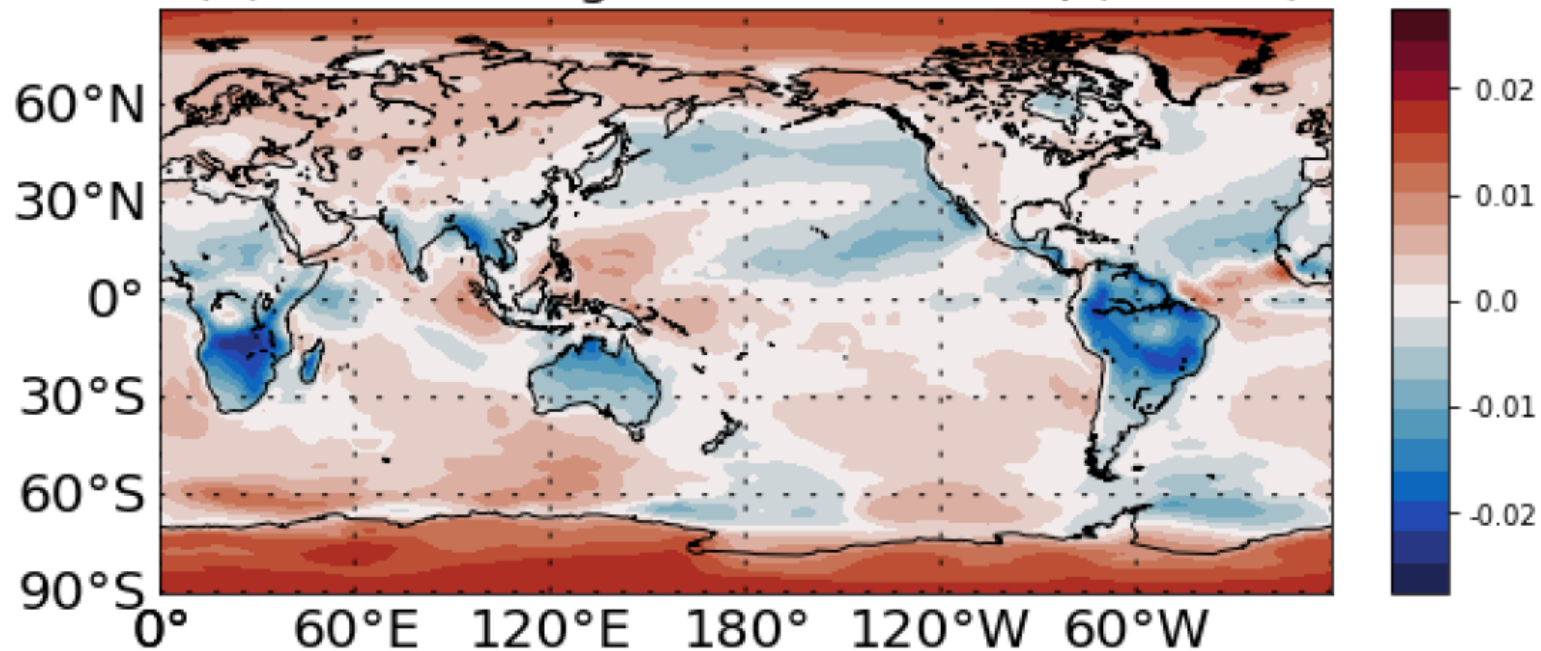


第三大本征微观态的主要特征：

ident. The 0.5-year period of EM3 follows the maximum solar forcing due to the sun crossing the equator twice a year, which is evident over the Indian Ocean. Meanwhile, due to the surface wind adjustment[23], the SAT and SST in the equatorial eastern Pacific and Atlantic exhibit a distinct annual cycle despite of the occurrences of the two equinoxes, which explains the 1-year period of EM3. Fig. 11(c) shows the time series of EM3. A robust upward trend is evident, implying the potential impact of global warming on the tropical SST and convective precipitation. It is interesting that a tipping in mid-1970s is detected by EM3. This is consistent with the well-known 1976-1977 climate shift [24].

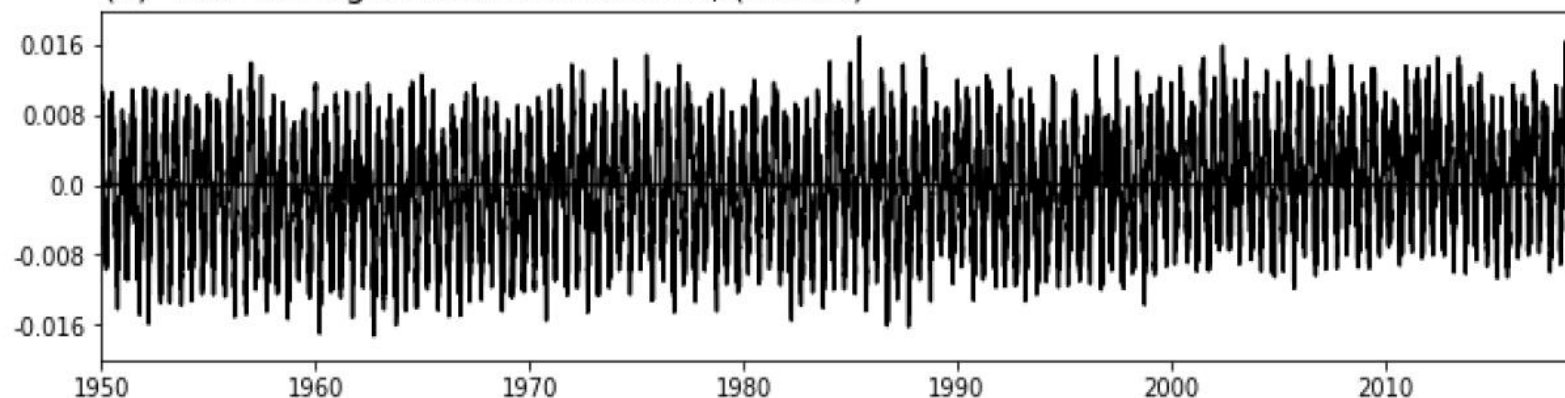
第四大本征微观态（非线性半年循环）

(d) The 4th eigen microstate \mathbf{U}_4 (2.13%)

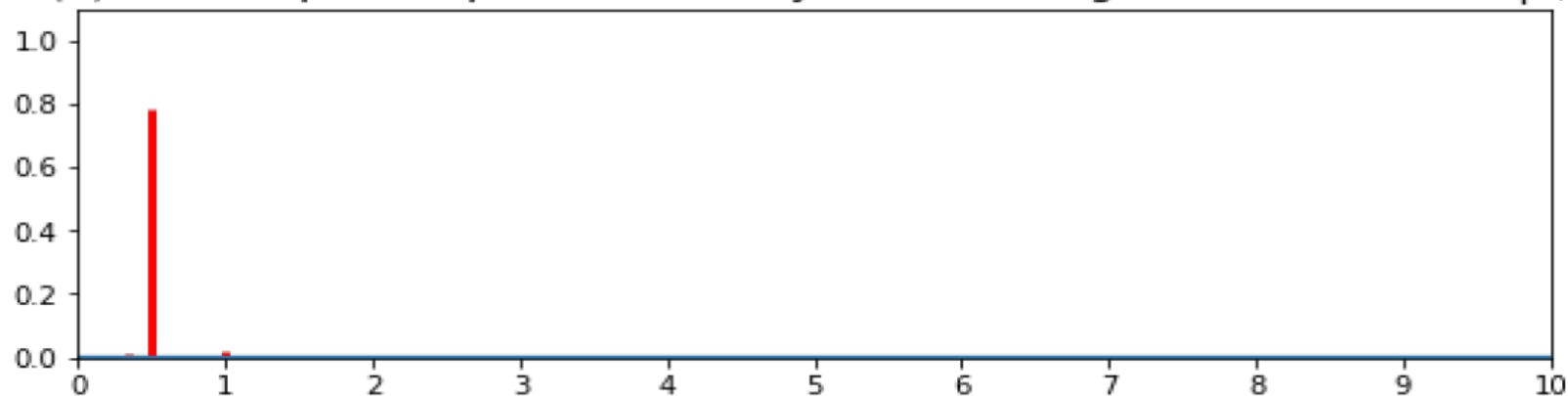


第四大本征微观态:

(d) The 4th eigen time evolution \mathbf{V}_4 (2.13%)



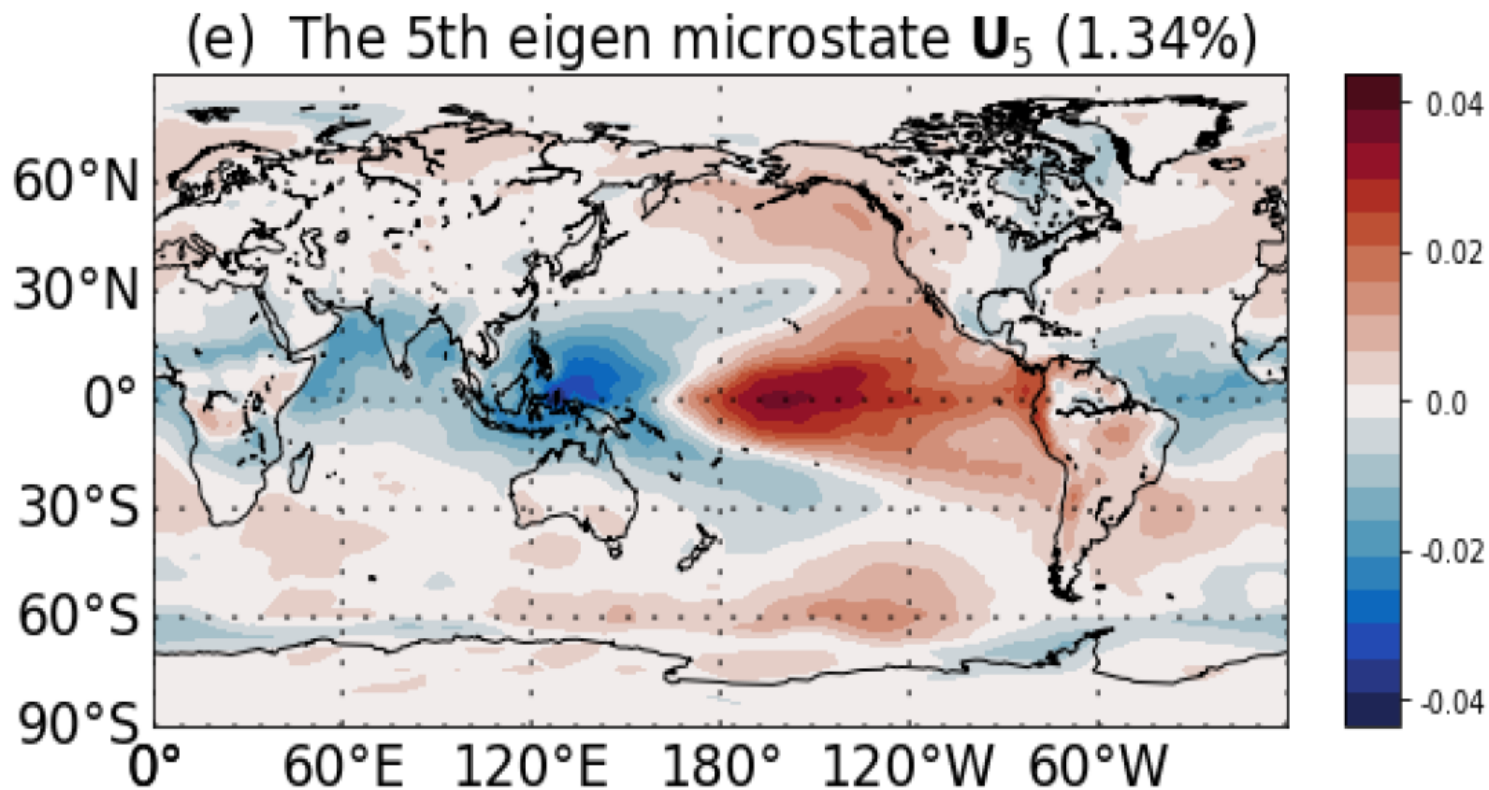
(d) Fourier power spectrum density of the 4th eigen time evolution $|\mathbf{V}_4|$



对应于气象学的半年振荡:

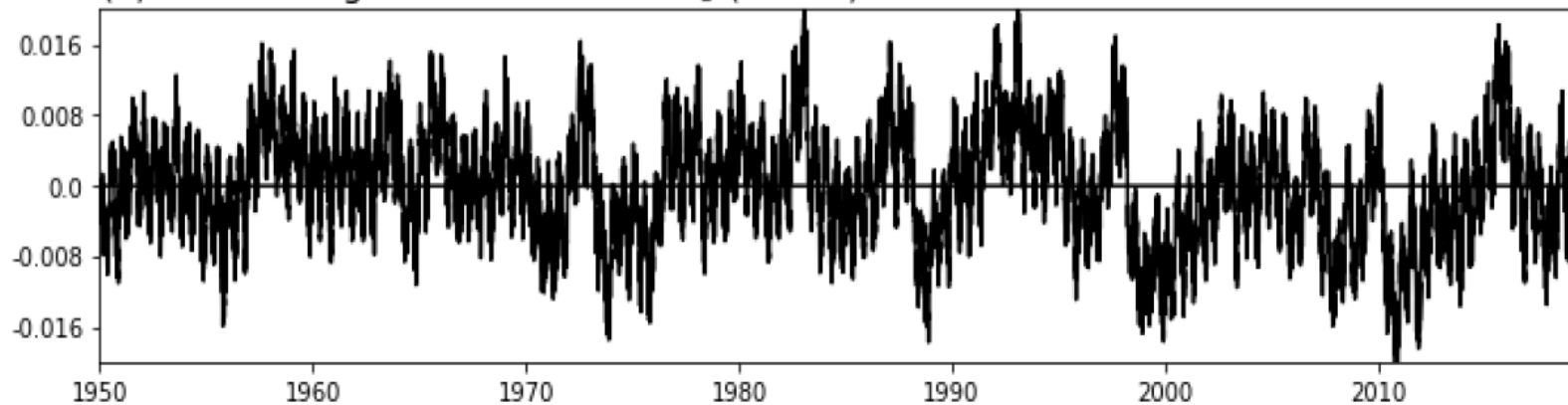
signal as the power spectrum showing (Fig. 12(d)). In meteorology, this semiannual signal is called semiannual oscillation (SAO), which is component of the annual cycle of a variable that consists of a sinusoidal oscillation with a period of six months [25]. Strong semiannual signals in thermal and momentum fields of the troposphere are found in both the Tropics and in Southern Hemisphere middle and high latitudes. The SAO is detectable as a significant contribution of the second harmonic to the annual march of temperature, surface air pressure, wind speed et al[26–29]; Here, we applied a harmonic analysis method called NMD to extract its second harmonic wave and showed its amplitude as seen in the Fig. 17(b), which is highly consistent with the results of Fig. 17(a), especially in Antarctic region. Previous studies have pointed out that the mechanism of SAO in Antarctic is mainly contributed to differ annual cycles of temperature in the mid-latitude ocean and Antarctic regions with the complex thermodynamics and dynamics of the SH ocean-atmosphere system [30–32].

第五大本征微观态（**EL-Nino/La** 现象）

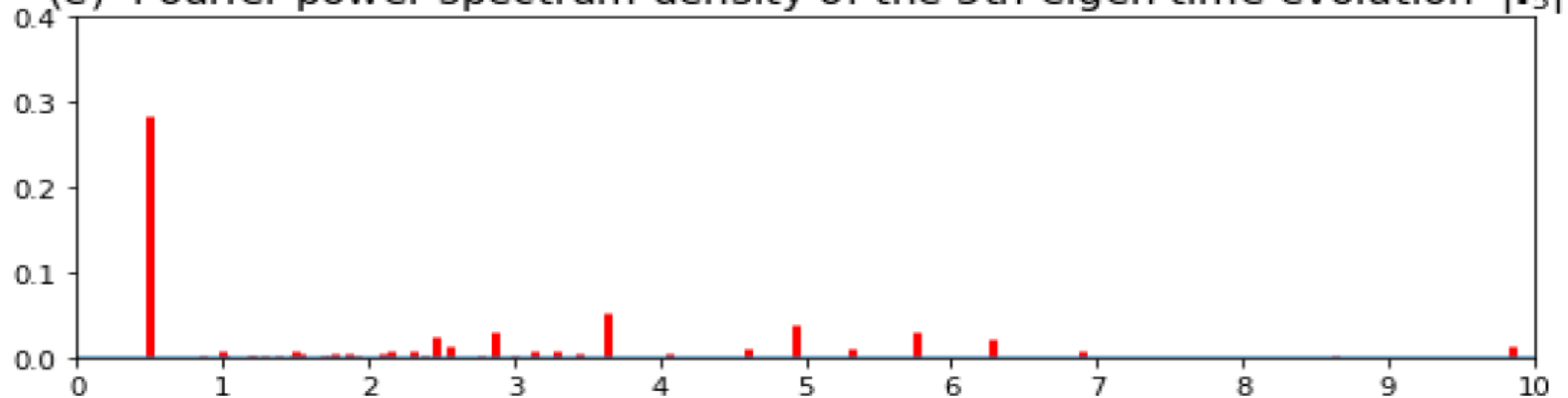


第五大本征微观态:

(e) The 5th eigen time evolution \mathbf{V}_5 (1.34%)

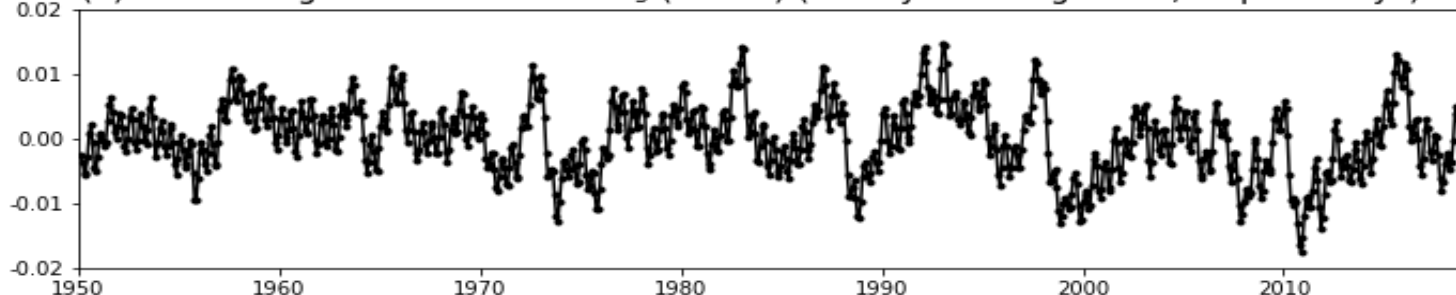


(e) Fourier power spectrum density of the 5th eigen time evolution $|\mathbf{V}_5|$

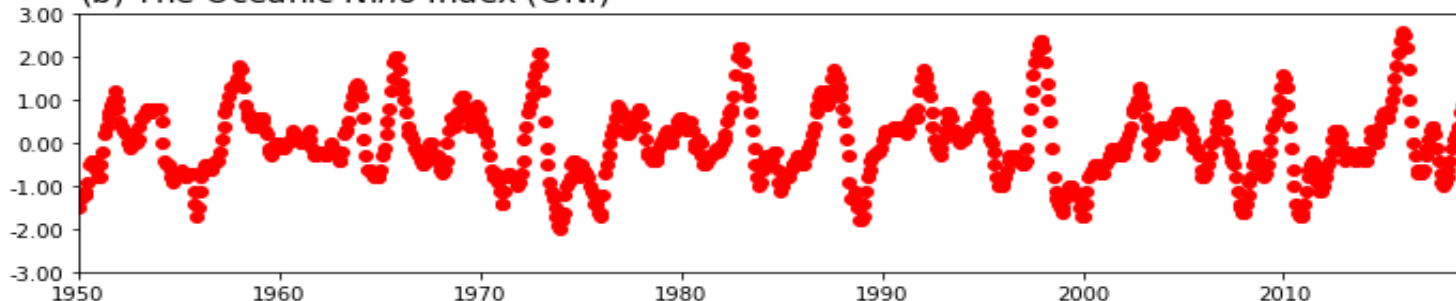


与厄尔尼诺指数的比较:

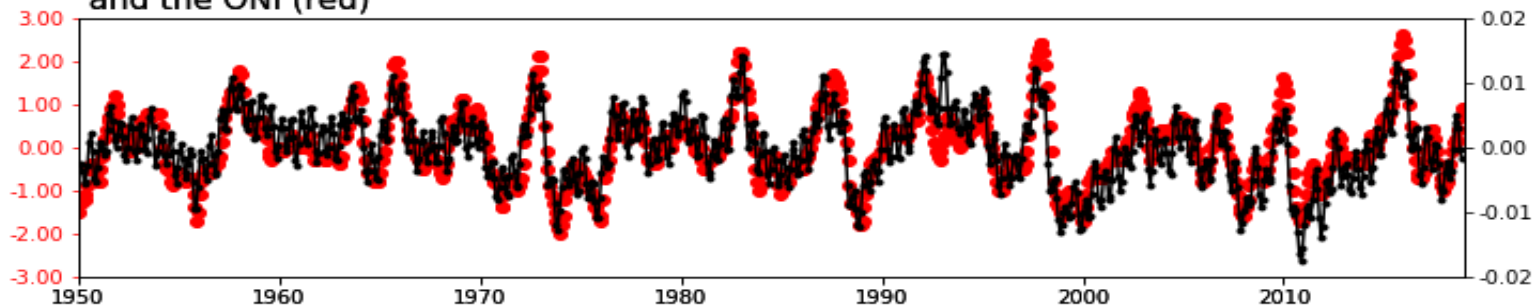
(a) The 5th eigen time evolution V_5 (1.06%) (90 days running mean, step: 30 days)



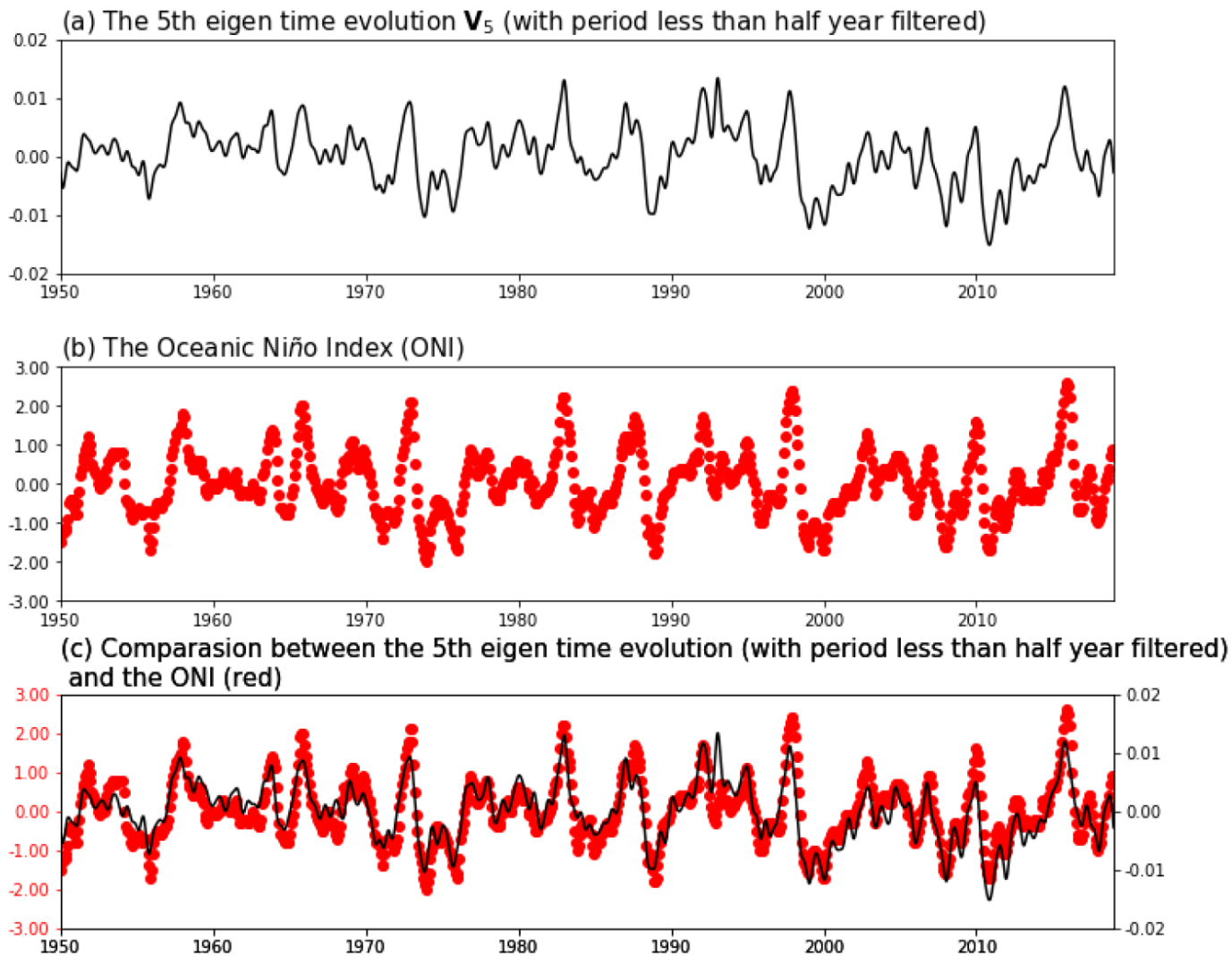
(b) The Oceanic Niño Index (ONI)



(c) Comparison between the 5th eigen time evolution (90 days running mean, step: 30 days, black) and the ONI (red)



与厄尔尼诺指数的比较:



对应于厄尔尼诺现象 (ENSO) :

the total variance. The most remarkable feature is evident over the tropical Pacific Ocean, with the warming over the central to eastern Pacific and cooling over the western Pacific. This pattern resembles the El-Niño and Southern Oscillation (ENSO), which is the strongest climate fluctuation at interannual time scale[33]. Spectrum analysis is conducted (Fig.12(e)). Other than the semi-annual cycle, the broad spectrum is evident at interannual time scale from 2 to 7 years in EM5, which is consistent with ENSO spectrum. Fig. 13 compares the time series in EM5 with the observed ONI index. Significant correlation of 89% is obtained after removing the semi-annual and higher frequency component. Three super El Niño events in 1982/1983, 1997/1998 and 2015/2016 are all detectable by EM5, further confirming the linkage between EM5 and ENSO. Further results (Fig. 18) show that the maximum of EM5 often occurs in November and the minimum of EM5 occurs in May after removing the semi-annual and higher frequency component.

金融系统的本征微观态:

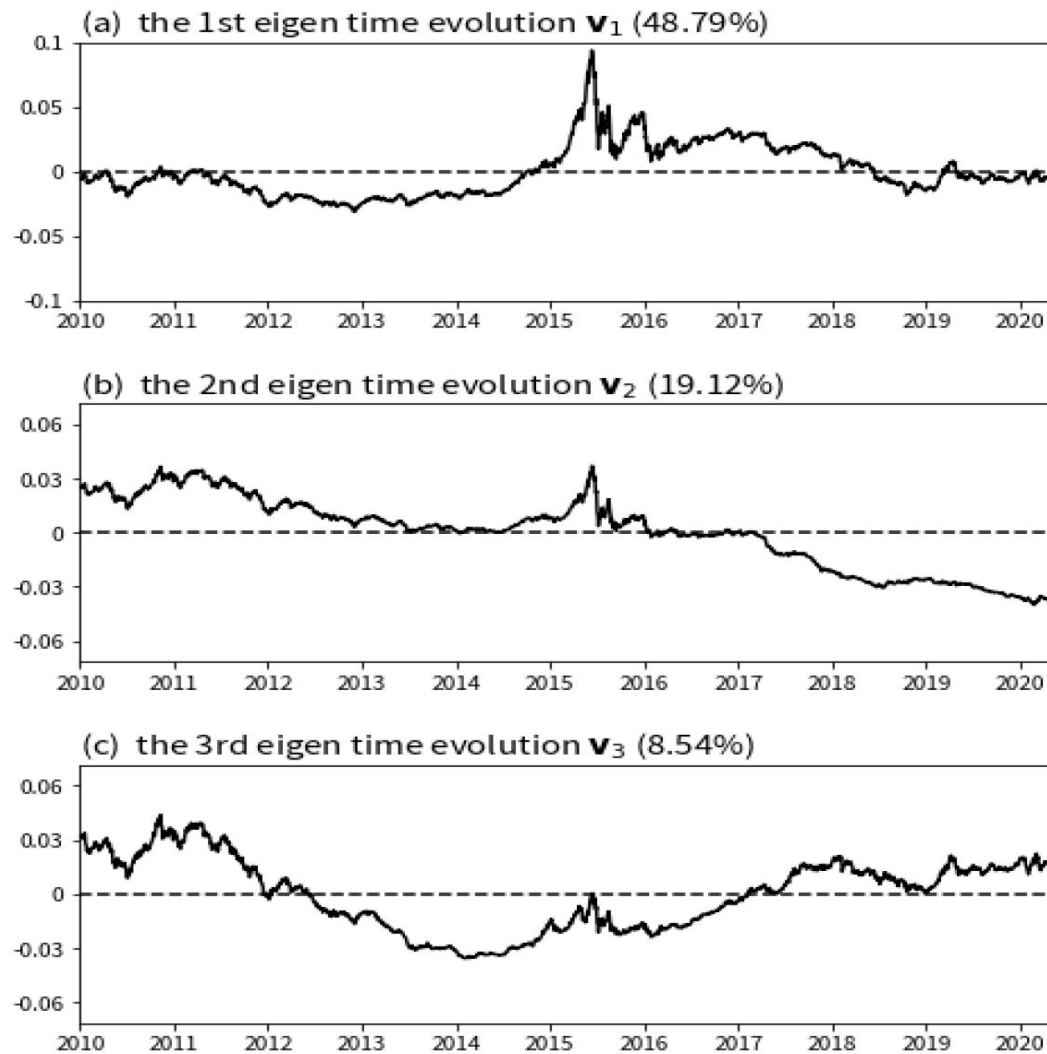
tional example. The fluctuation of the stock price from 2010-1-4 to 2020-5-26 in Chinese mainland is studied. The data comes from the public data published by Shanghai Stock Exchange and Shenzhen Stock Exchange. After removing the stocks in the special treatment state, there are 1460 mainland-listed stocks left in the dataset. At time t , the price of the stock i can be denoted by $P_i(t)$. The average price of the stock i during the specified period can be calculated as

$$\langle P_i \rangle = \frac{1}{M} \sum_{t=1}^M P_i(t). \quad (43)$$

At any time t , the price fluctuation of the stock i

$$\delta P_i(t) = P_i(t) - \langle P_i \rangle. \quad (44)$$

三大本征微观态的时间演化:



第一大本征微观态与上证100指数的比较:



FIG. 24. Comparison between the U_1 in the stock price fluctuation ensemble (black line) and the SSE100 Index (red line).

第二大本征微观态与能源行业指数的比较:



FIG. 25. Comparison between the U_2 in the stock price fluctuation ensemble (black line) and the SSE Energy Sector Index (red line).

第三大本征微观态与材料行业指数的比较:



FIG. 26. Comparison between the U_3 in the stock price fluctuation ensemble (black line) and the SSE Materials Sector Index (red line).

漏斗颗粒流速度场的标度性

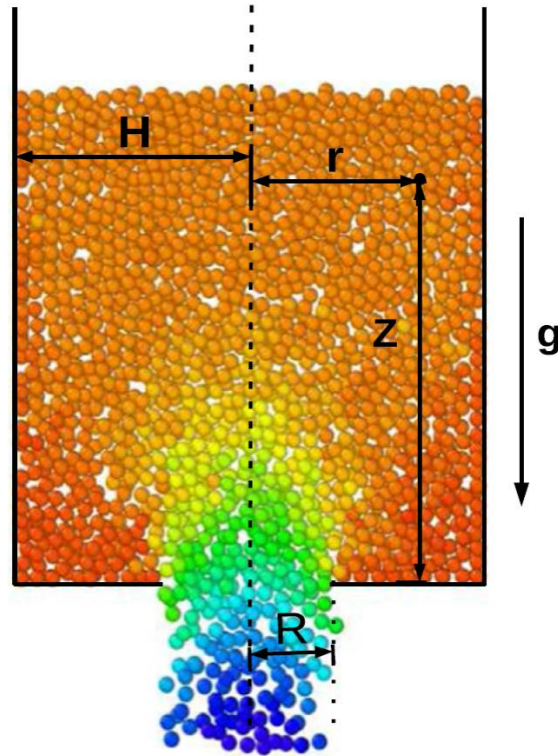



Fig. 1 Schematic diagram of granular flow through an aperture

颗粒物质的例子



特征

- 颗粒尺度 1微米 — 10^4 m
- 势能 mgd / KT  可忽略温度的影响
- 相互作用：硬球 + 短程力，
重力，摩擦力，碰撞

离散介质，非线性体系，能量耗散

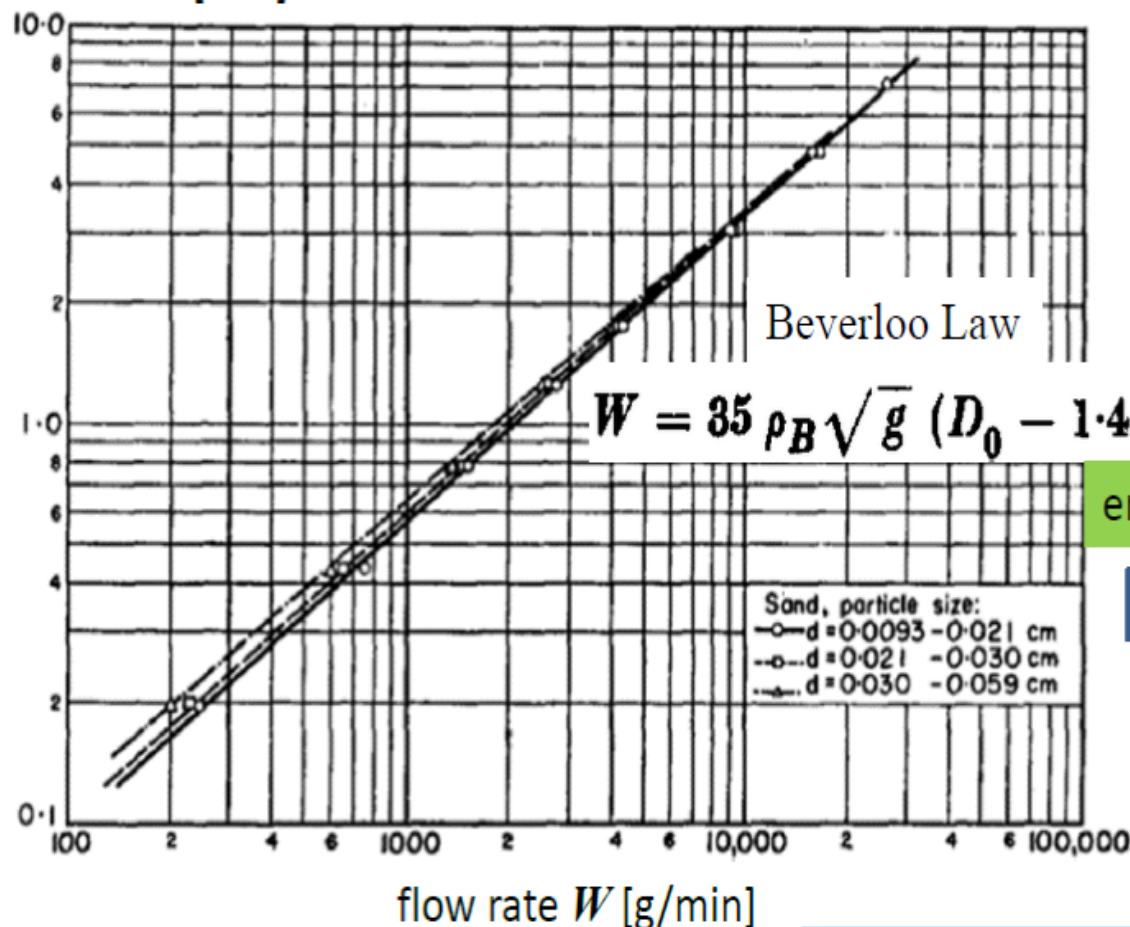
The flow of granular solids through orifices

Chemical Engineering Science, 1961, Vol. 15, pp. 260 to 269

W. A. BEVERLOO, H. A. LENIGER and J. VAN DE VELDE

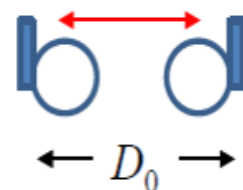
Technological Laboratory, Agricultural University, Wageningen, Netherlands

exit area [cm²] $\sim d^2$



dimensional analysis

empty annulus



empirical results from experimental data

Beverloo Law (1961)

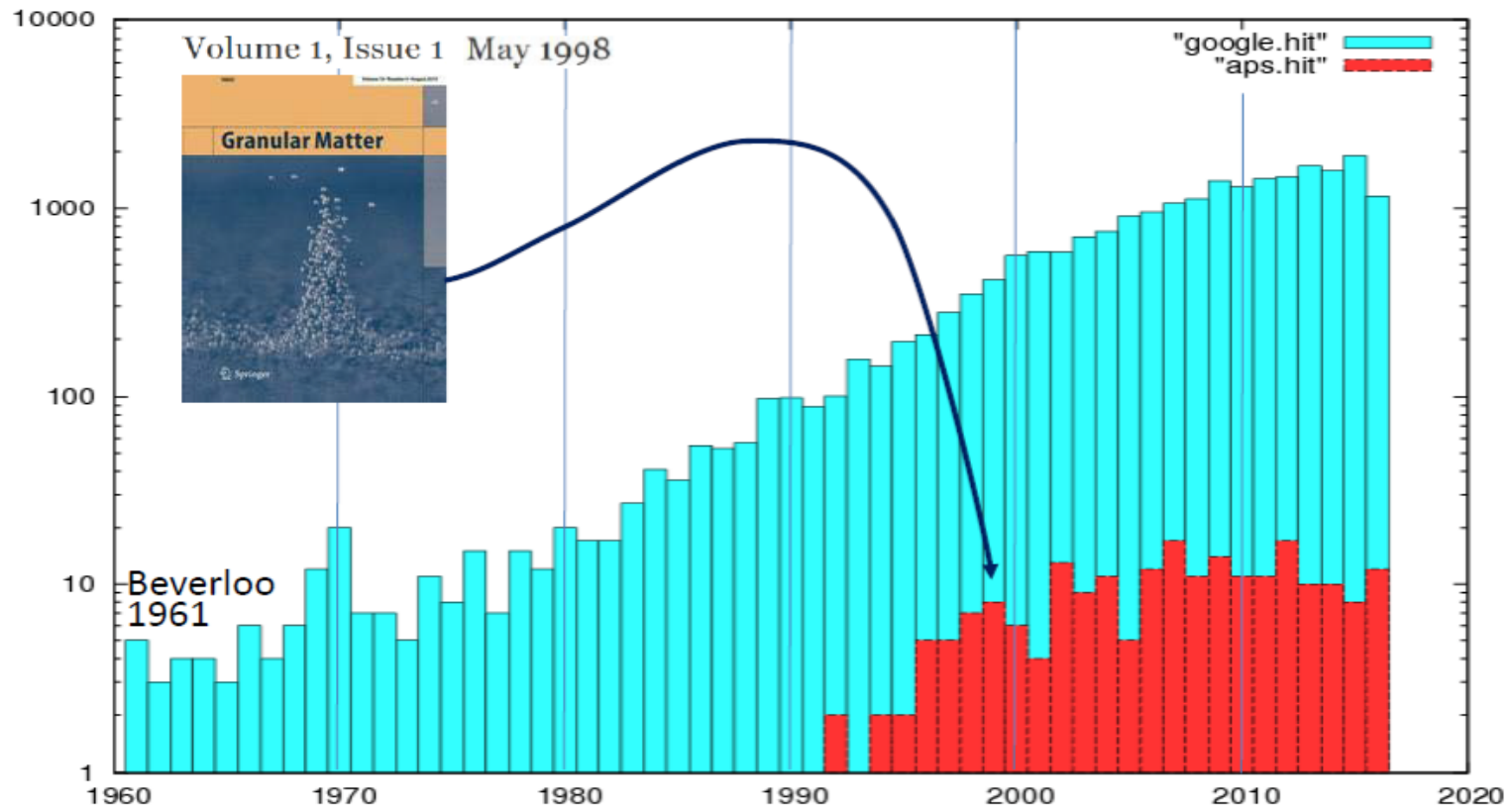
$$W = C\rho\sqrt{g}(R - kd)^{D-\frac{1}{2}}, \quad (1)$$

where g is the gravitational acceleration, ρ is the bulk density, R is the orifice radius, d is the diameter of granule, and D is the dimensionality, respectively. C and k are two fitted parameters. The Beverloo law was re-

Research in granular flow

Search on <http://scholar.google.com.tw/>
and <http://journals.aps.org/>
using "granular flow"

Number of hit



Free fall arch

R. L. Brown, *Nature* 191, 458 (1961).

B. P. Tighe and M. Sperl, *Granular Matter* 9, 141 (2007).

实验否定了Free fall arch的存在

Disentangling the Free-Fall Arch Paradox
in Silo Discharge

S. M. Rubio-Largo, A. Janda, D. Maza,
I. Zuriguel, and R. C. Hidalgo

Phys. Rev. Lett. 114, 238002 – Published
11 June 2015

颗粒流速度场的尺度标度关系

Granular Matter (2019) 21:21

<https://doi.org/10.1007/s10035-019-0872-z>

ORIGINAL PAPER

Size scaling relation of velocity field in granular flows and the Beverloo law

Gaoke Hu^{1,4} · Ping Lin² · Yongwen Zhang^{1,4} · Liangsheng Li³ · Lei Yang² · Xiaosong Chen^{1,4} 

Received: 20 September 2018

© Springer-Verlag GmbH Germany, part of Springer Nature 2019

速度场的尺度标度关系

we propose a size scaling relation of vertical velocity field as

$$v_z(r, z; R)/v_z(0, 0; R) = f(r/R_r, z/R_z), \quad (2)$$

where $R_r = R - 0.5d$ is the effective aperture radius and $R_z = R - k_2d$ is a vertical length scale to be determined.

有效加速度

During a time period δt , granules at position (r, z) move in average to another position $(r, z + v_z(r, z; R)\delta t)$. Their average vertical velocity has a change $\delta v_z = v_z(r, z + v_z(r, z; R)\delta t; R) - v_z(r, z; R)$ during δt . An effective acceleration can be calculated as

$$a_{\text{eff}}(r, z; R) \equiv \lim_{\delta t \rightarrow 0} \frac{\delta v_z}{\delta t} = \frac{\partial v_z(r, z; R)}{\partial z} v_z(r, z; R) . \quad (3)$$

有效加速度的尺度标度

According to the size scaling relation of $v_z(r, z; R)$ in Eq. (2), we obtain

$$a_{\text{eff}}(r, z; R) = \left[v_z^2(0, 0; R) / R_z \right] \theta(r/R_r, z/R_z) , \quad (4)$$

where the scaling function

$$\theta(\bar{r}, \bar{z}) = f(\bar{r}, \bar{z}) f_z^{(1)}(\bar{r}, \bar{z}) , \quad (5)$$

边界条件

At the center of aperture, the effective acceleration

$$a_{\text{eff}}(0, 0; R) = \left[v_z^2(0, 0; R) / R_z \right] \theta(0, 0). \quad (6)$$

In the asymptotic case that $H \gg R$ and $R \gg d$, the granules at the center of aperture are assumed to fall freely. Then the effective acceleration has the boundary condition

$$a_{\text{eff}}(0, 0; R) = -g, \quad (7)$$

which results in

$$v_z(0, 0; R) = \sqrt{-g / \theta(0, 0)} R_z^{1/2} \quad (8)$$

with $\theta(0, 0) = f_z^{(1)}(0, 0)$.

Beverloo定律

The mass flow rate W of D -dimensional hopper can be calculated as

$$W = \int_0^{R_r} \rho v_z(r, 0; R) S_{D-1} r^{D-2} dr. \quad (9)$$

We have $S_1 = 2$ in two-dimensional and $S_2 = 2\pi$ in three-dimensional hoppers. Using the size scaling relation of $v_z(r, z; R)$ and the boundary condition at $r = 0$ and $z = 0$, we can obtain

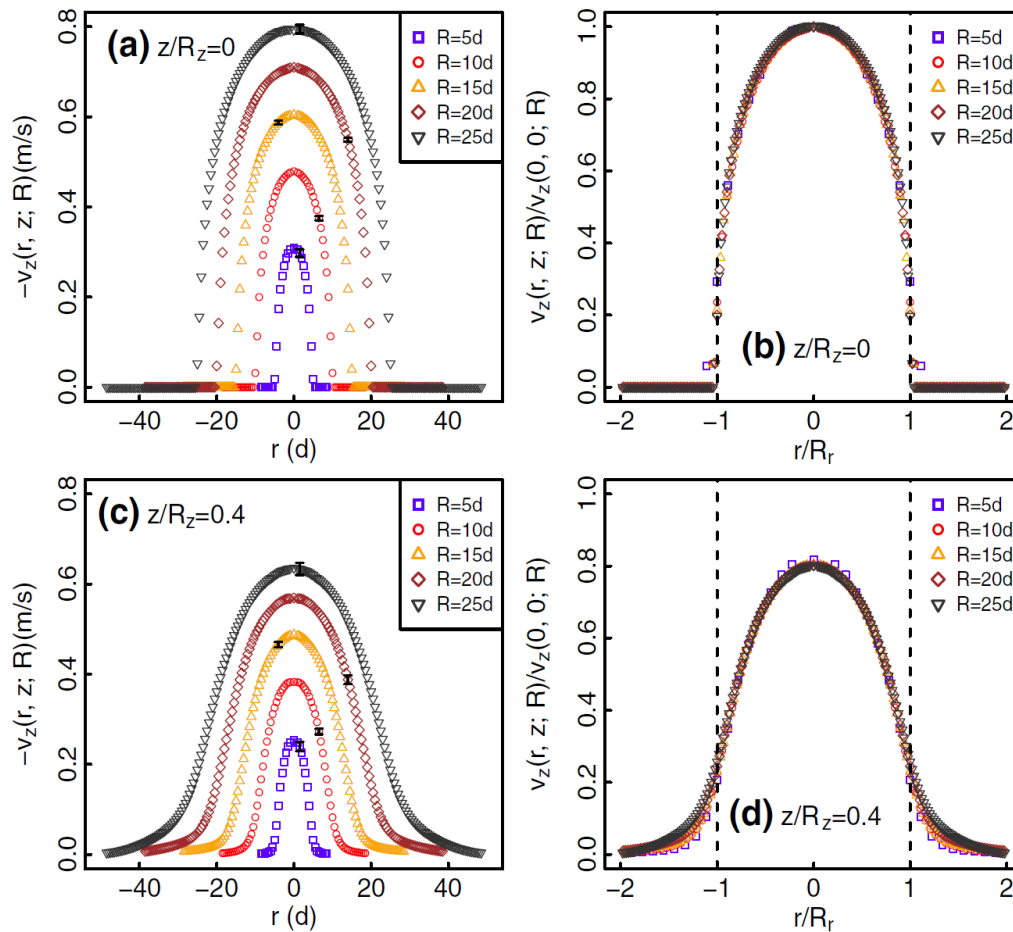
$$W = C_1 \rho \sqrt{g} (R - 0.5d)^{D-1} (R - k_2 d)^{1/2}, \quad (10)$$

where $C_1 = S_{D-1} [-f_z^{(1)}(0, 0)]^{-1/2} \int_0^1 f(x, 0) x^{D-2} dx$. In the limit $R \gg d$, our result becomes $W \simeq C_1 \rho \sqrt{g} R^{D-\frac{1}{2}}$ and is in agreement with the Beverloo law.

速度场尺度标度关系的计算模拟检验

We simulate granular flows both in 3D and 2D hoppers in order to test the size scaling relation in general dimension. In the 3D hopper with radius $H = 60d$, there are $N = 4,400,000$ granules which flow through the apertures with radii $R = 5d, 10d, 15d, 20d, 25d$. We take the snapshots of granules with their positions and velocities every 100,000 steps with a step $\tau = 5.0 \times 10^{-7}$ s. In the 2D hoppers with radius $H = 100d$, we use $N = 200,000$ granules which flow through the apertures with radii $R = 8d, 10d, 15d, 20d, 25d$. The snapshots of granules with their positions and velocities are taken every 20,000 steps.

速度场尺度标度性的检验



结论:

- 利用实验测量或计算模拟数据可定义复杂系统的微观态，从而得到该系统的统计系综
- 利用微观态关联矩阵的本征矢量，可得到本征微观态，以及它随时间的演化。本征微观态之间无关联，原始微观态可看作本征微观态的叠加，其权重与本征值成正比。
- 当某个本征微观态的权的热力学极限趋于有限，如同玻色-爱因斯坦凝聚，系统发生相变，序参量由本征值描述，新相由本征微观态表征
- 不同维数Ising模型的计算模拟结果完全证实了本征微观态理论。应用于地球系统温度涨落，获得了气候学意义非常重要的不同本征微观态。

结论:

- 提出了漏斗颗粒流（漏斗口附近）速度场的尺度标度性，由此可自然得到著名的Beveloo定律。
- 速度场的尺度标度性得到了计算模拟的完全证实

致谢：

合作者：胡高科，孙宇（中科院理论物理研究所）
张永文（巴依兰大学，以色列）
樊京芳（PIK, 德国）
陆征辉（中科院大气物理所）
陆波（中国气象局 国家气候中心）
邓琪敏（北京大学物理学院）

颗粒流：杨磊（中科院兰州近代物理研究所）
林平（中科院兰州近代物理研究所）